Title: Dopaminergic control of postnatal mammalian spinal network function is predominantly inhibitory

Abbreviated title: Dopamine receptor mechanisms of spinal modulation

Authors: Simon A. Sharples[1,2], Nicole E. Burma[1,2], Joanna Borowska-Fielding[3], Charlie H.T. Kwok[1,4], Shane E.A. Eaton[1,4], Glen B. Baker[5], Celine Jean-Xavier[4], Ying Zhang[3], Tuan Trang[1,4], Patrick J. Whelan[1,4]

Affiliations : [1] Hotchkiss Brain Institute, University of Calgary, Calgary, AB, Canada, T2N4N1, [2]Department of Neuroscience, University of Calgary, Calgary, AB, Canada, T2N 4N1, [3] Department of Medical Neuroscience, Dalhousie University, Halifax, NS, Canada, B3H 4R2.[4] Department of Comparative Biology and Experimental Medicine, University of Calgary, Calgary, AB, Canada, T2N4N1, [5] Department of Psychiatry (NRU), Faculty of Medicine and Dentistry, University of Alberta, Edmonton, AB, Canada. T6G 2G3.

Correspondence:
Dr. Patrick Whelan
HMRB 168
3330 Hospital Drive NW
Calgary, Alberta, Canada, T2N 4N1
whelan@ucalgary.ca

Number of pages: 53
Number of Figures: 9
Number of Tables: 2
Word Count: Abstract, (247) Introduction (641), Discussion (1500)

Acknowledgments: We would like to acknowledge support from the Whelan Lab and technical support from Dr. Heather Leduc-Pessah and Rebecca Dalgarno on immunoprecipitation experiments and from Gail Rauw on HPLC experiments. Spinalcore software was a kind gift from Prof A. Lev-Tov (Hebrew University).

Funding: We acknowledge studentships from the Natural Sciences and Engineering Research Council of Canada (SAS: NSERC-PGS-D), the Canadian Institute for Health Research (NEB, YZ), Alberta Innovates - Health Solutions (AIHS: SAS, NEB), Hotchkiss Brain Institute (SAS, NEB) and the Faculty of Veterinary Medicine (CHTK). This research was supported by grants to PJW provided by the Canadian Institutes of Health Research and NSERC (Discovery grant).

Contributions: SAS performed and analyzed whole-cell and network electrophysiology, NEB, performed and analyzed CoIP, GBB performed and analyzed HPLC, JBF performed recordings from V3 interneurons and SAS, CHTK and SEAE performed IHC and imaging experiments. SAS, CJ-X and PJW interpreted results. SAS prepared figures and drafted the manuscript. TT, YZ and PJW contributed to experimental design and procured funding. SAS, CJ-X and PJW conceived and designed the research. All authors reviewed and approved the final version of the manuscript.

Abstract

At birth, descending pathways are still maturing and spinal networks function at a lower excitability state characterized by spontaneous activity. The effects of monoamines, however, are typically examined when spinal networks are in high excitability states when drug-evoked locomotor activity is induced. A gap in our knowledge is how monoamines affect neonatal spinal networks under more physiological, low-state, conditions. Here, we explored receptor and cellular mechanisms mediating dose-dependent control of dopamine on spinal motor networks of the neonatal mouse in vitro. During a low excitability state, low concentrations of dopamine suppressed spontaneous activity by acting on D_2, D_3, D_4 and α_2-adrenergic receptors in parallel. Network inhibition was reproduced by blocking dopamine reuptake and metabolism to augment endogenous dopamine levels. Activation of D_2 receptors hyperpolarized a subset (33%) of ventral interneurons, but not motoneurons. Similar proportions of descending commissural and V3 interneurons were hyperpolarized indicating that D_2 actions are not localized to particular classes of interneurons consistent with the kernel of the locomotor central pattern generator being distributed across several interneuronal classes. High concentrations of dopamine produced excitatory effects mediated mainly by a D_1 receptor-mediated increase in motoneuron excitability. High concentrations of dopamine also increased spinal network activity by co-activating D_1 and D_2 receptors. Our data indicate that the actions of neuromodulators are codependent on their receptor targets and the network state. Under low excitability states, our findings also explain how receptor and cellular mechanisms contribute to the diverse, concentration-dependent control of spinal networks in the neonatal mouse.

Keywords: dopamine, dopamine receptors, spinal cord, rhythmicity, motor systems

Significance statement: Monoaminergic neuromodulation of neural networks is dependent not only on target receptors but also on network state. We studied the dose-dependent control of spinal networks of the neonatal mouse, in vitro, during a low excitability state characterized by spontaneous network

activity. Spontaneous activity is an essential element for the development of networks. Under these conditions, we defined converging receptor and cellular mechanisms that contribute to the diverse, dose-dependent control of spinal motor networks by dopamine, in vitro. These experiments advance understanding of how monoamines modulate spinal motor function under dynamically changing excitability conditions.

Introduction (641 words)

Neuromodulators are critical for central nervous system function and create diverse circuit output by altering synaptic and intrinsic properties (Marder and Thirumalai, 2002; Stein, 2009; Miles and Sillar, 2011). The magnitude and direction of neuromodulatory effects are dictated by network state (Gutierrez et al., 2013; Marder et al., 2014), a concept which is especially important in developing spinal motor networks. This is because spinal networks produce a wide repertoire of patterned outputs at birth including locomotor activity. That being said, neonatal rodents rarely produce coordinated bouts of locomotion and in vitro preparations of isolated spinal cord require pharmacological or electrical stimulation to drive the network into a high excitability state to produce fictive walking patterns (Smith and Feldman, 1987; Jiang et al., 1999; Whelan et al., 2000a). Instead, the vast majority of movements observed in neonatal mice are ataxic. (See Supplementary Video 1). These movements correlate with spontaneous network activity, which can be observed in vitro (Bonnot et al., 1998; Dalrymple et al., 2019). Little is known about how neuromodulators regulate this activity which is important because spontaneous activity is critical for the maturation of spinal networks during embryonic and early postnatal development (Hanson and Landmesser, 2003, 2004; Ren and Greer, 2003; Myers et al., 2005; Warp et al., 2012).

Dopamine is a key neuromodulator that regulates spinal sensory and motor circuits (McPherson and Kemnitz, 1994; Schotland et al., 1995; Garraway and Hochman, 2001; Barriere et al., 2004; Madriaga et al., 2004; Zhu et al., 2007; Lapointe et al., 2009; Musienko et al., 2011; Clemens et al., 2012; Humphreys and Whelan, 2012; Lambert et al., 2012; Gozal et al., 2014; Sharples et al., 2015; Picton and Sillar, 2016; Picton et al., 2017; Sharples and Whelan, 2017; Megat et al., 2018) and in larval zebrafish alters spinal network architecture (Reimer et al., 2013) and function leading to changes in locomotor behaviour (Lambert et al., 2012). Phasic and tonic firing of descending dopaminergic neurons correlates with locomotor episodes and quiescence in larval zebrafish, respectively (Jay et al., 2015); however, less is

known about the effects of dopamine in mammals. Different firing patterns impact cellular release of dopamine and the receptor subtypes it activates (Dreyer et al., 2010). Since all dopamine receptors are expressed in rodent lumbar spinal cords (Zhu et al., 2007), high levels of dopamine released during phasic cell firing should activate lower affinity excitatory D_1 receptors and promote locomotor activity, and lower levels of dopamine released during tonic activity should activate higher affinity inhibitory D_2 receptors and suppress motor output. Consistent with this notion, dopamine has dose-dependent effects on locomotor circuits in precocial species with functional swim networks (Clemens et al., 2012). In contrast, altricial species, such as mice, have lumbar locomotor networks that rarely generate coordinated movements at birth and instead generate spontaneous activity characteristic of immature networks operating in a low excitability state. We have previously demonstrated that neuromodulation of mammalian spinal networks is linked to ongoing network excitability state (Sharples and Whelan, 2017). Based on our previous work, we hypothesized that receptor actions, and therefore dose-dependent control of network output by dopamine, is linked to the underlying network excitability state (Sharples and Whelan, 2017) and that more complex actions may have been masked during high excitability states of fictive locomotion.

Our findings demonstrate that dose-dependent dopaminergic control of spinal network function is diverse during low excitability states characterized by spontaneous network activity. We demonstrated, for the first time to our knowledge, a link between receptor and cellular mechanisms that contribute to the diverse actions that dopamine exerts on spinal motor networks. While the excitatory D_1 system is functional at birth, at this stage in development, endogenous dopamine acts to dampen the excitability of the spinal motor system by activating D_2 receptors. Portions of these data were presented in abstract form (Sharples and Whelan, 2015; Sharples et al., 2017).

Results

Dopaminergic modulation of spinal motor networks is dose-dependent and bidirectional

We focused on the modulation of perinatal spontaneous activity patterns to investigate how dopamine modulates spinal network output during a physiologically relevant low excitability state. Using the same configuration as Sharples et al. (2015), we recorded spontaneous motor activity with extracellular suction electrodes from single ventral roots of the second or fifth lumbar (L2/L5) segments simultaneously from two or four spinal cord preparations sharing the same chamber. Each preparation in this series of experiments was naïve to dopamine exposure and received only a single dose of its respective concentration. This configuration ensured consistent experimental conditions across several preparations exposed to different concentrations of dopamine. Low concentrations of dopamine (1–30 μM) consistently suppressed spontaneous motor activity, whereas higher concentrations (100–300 μM) excited spontaneous motor activity, evoking episodic and continuous rhythmic patterns (Fig. 1; $n = 42$, $F_{(5,36)} = 10.5$. $p < 0.001$).

Parallel actions of D_2, D_3, D_4, dopamine and alpha-2 adrenergic receptors mediate dopaminergic inhibition of spontaneous activity

To delineate receptor contributions to dopamine's bidirectional effects on endogenous spontaneous activity in isolated spinal cord preparations, we used antagonists selective for the family of dopamine receptors. At low concentrations of dopamine we observed a negative response ratio (Fig. 2A, Di), which was due to a reduction in the number (Fig. 2Dii), but not the amplitude, of spontaneous episodes (Fig. 2Diii). In contrast to our hypotheses, the inhibitory effect of dopamine at low concentrations (10 μM) was not altered by antagonists targeting D_2 (L-741,626; $n = 3$, response ratio = -0.57 ± 0.26), D_2/D_3 (sulpiride; 20 μM; $n = 10$, response ratio = -0.36 ± 0.2), D_3 (SB-27701-A, 5 μM; $n = 3$; response ratio = -0.36 ± 0.3), D_4 (L-745,870; $n = 3$, response ratio = -0.32 ± 0.1) or D_1/D_5 receptors (SCH 23390; $n = 4$, response ratio = -0.43 ± 0.2). However, when all D_2-like receptors were blocked with a cocktail of

sulpiride (D_2/D_3, 20 μM) and L-745,870 (D_4, 5 μM), response ratios indicated that the inhibitory effect of 10 μM dopamine was attenuated, compared with dopamine alone (Fig. 2C; n = 6; one-way analysis of variance (ANOVA), $F_{(4,32)} = 7.3$, $p < 0.001$; Tukey post hoc $p = 0.09$), to a level where it was not significantly different from a time-matched vehicle control (Fig. 2C, Di.; n = 6, $F_{(4,32)} = 7.3$, $p < 0.001$; Tukey post hoc, $p = 0.98$). Burst analysis revealed no difference in the number or amplitude of episodes when antagonists were present, compared with baseline (Fig. 2Dii, Diii; two-way ANOVAs for number, $F_{(2,28)} = 9.5$, $p < 0.0001$; two-way ANOVA for amplitude: $F_{(4,28)} = 3.4$, $p = 0.023$). Together these data suggest that the inhibitory actions of dopamine depend on parallel action of D_2, D_3 and D_4 receptors.

We considered the possibility that the inhibitory influence of low dopamine concentrations was partly due to the activation of non-dopamine receptors. Previous work conducted in our laboratory showed that dopamine inhibits cauda equina-evoked locomotion, partially via α_2-adrenergic receptors (Gordon and Whelan, 2006). The remaining minor inhibitory effect of dopamine at 10 μM was blocked by antagonizing the α_2-adrenergic receptors with yohimbine (4 μM) in the presence of D_2/D_3 and D_4 receptor antagonists. We observed significantly different response ratios, compared with 10 μM dopamine alone (Fig. 2Di; n = 6, $F_{(4,32)} = 7.3$, $p < 0.001$; Tukey post hoc, $p = 0.006$). Low dopamine concentrations did not change the number or amplitude of episodes in the presence of these antagonists, compared with baseline (Fig. 2Dii, Diii) suggesting that non-dopamine receptors also contribute to dopamine's inhibitory effects.

D_1 - D_2 receptor coactivation contributes to dopaminergic excitation of spinal network activity

Dopamine binding to D_1 and D_2 heteromers can lead to depolarization via an increase in intracellular calcium levels, mediated by the enzyme phospholipase C (PLC) (LaHoste and Marshall, 1993; Lee et al., 2004; Rashid et al., 2007; Thompson et al., 2016). Thus, we first tested the role of the lower affinity D_1 receptor system and then examined whether the D_2 receptor system has a cooperative role in the control of spontaneous activity. With the addition of dopamine at high concentrations (i.e., 50 & 100 μM),

spontaneous activity patterns became rhythmic, often producing a slow rhythm with episodes of high frequency rhythmic activity. Moreover, the presence of the D_1-like receptor antagonist, SCH-23390, reduced this effect (Fig. 3; 100 μM dopamine with 10 μM SCH-23390; n = 5; response ratio, $F_{(5,35)}$ = 11.4, $p < 0.001$); fast rhythm power, $F_{(4,27)} = 12.6$, $p < 0.001$; slow rhythm power, $H_{(4)} = 12.8$, $p = 0.013$; Fig. 3 B & C, 50 μM dopamine with 10 μM SCH-23390; response ratio, $F_{(5,35)} = 11.4$, $p < 0.001$; fast rhythm power, $F_{(4,27)} = 12.6$, $p < 0.001$; slow rhythm power, $H_{(4)} = 12.8$, $p = 0.013$, Dunn's post hoc: $p = 0.03$; one way ANOVA used in tests). These results suggest that the excitatory effects of dopamine are primarily mediated by the D_1-like receptor family.

If D_2 receptors form heteromers with D_1 receptors, we would expect that antagonists would inhibit, rather than excite responses. We tested this idea by administering D_2-like antagonists (sulpiride + L745,870) and found that the power of the fast rhythm elicited by dopamine at 100 μM was reduced (Fig. 3 Aiii, Biii, Cii; n = 4; $F_{(4,27)} = 12.6$, $p < 0.001$) to the same extent as the D_1-antagonist, with no effect on the power of the slow rhythm (Fig. 3Ciii; $H_{(4)} = 12.8$, $p = 0.013$; Dunn's post hoc, $p = 1.0$). This suggests that D_2 receptors may contribute to the excitatory effects of dopamine.

To explore the interaction and co-activation profile of D_1 and D_2 receptors in isolated neonatal spinal cords, we performed co-immunoprecipitation for D_1 and D_2 receptors and used agonists to activate both receptor subtypes. After immunoprecipitating D_2 receptors from neonatal spinal cord lysates, we used an antibody to probe for D_1 receptors. We detected D_1 receptor protein within the D_2 receptor immunoprecipitates (Fig. 4Ciii), indicating that D_1 and D_2 receptors form a protein complex in neonatal mouse spinal cords.

In support of this idea, co-application of the D_1 agonist SKF 81297 (50 μM) and the D_2 agonist quinpirole (50 μM) elicited a more robust depolarization of the ventral root DC potential, compared with 50 μM of the D_1 agonist alone (Fig. 4A, Ci; D_1, n = 8; D_1/D_2, n = 8; one-way ANOVA $F_{(2,21)} = 5.2$, $p = 0.01$; Tukey

post hoc: $p = 0.02$). We observed no difference in the amount of spontaneous network activity evoked with co-application of a D_2 agonist, compared with application of the D_1 agonist alone, as indicated by the response ratio (Fig. 4B, Cii; one-way ANOVA, $F_{(3,29)} = 12.0$, $p < 0.001$; Tukey post hoc, $p = 0.5$). In contrast, lower concentrations of the same agonists (10 μM) produced no effects ($n = 8$ for each condition; DC potential, $t_{(6)} = 0.73$, $p = 0.24$; response ratio, $t_{(6)} = 0.9$, $p = 0.19$). Thus, consistent with previous reports for striatal neurons (Lee et al., 2004), we found a dose-dependent effect of dopamine agonists wherein co-applying high doses, but not low doses, of D_1 and D_2 receptor agonists, produced more robust depolarization than a D_1 agonist alone.

In addition to co-applying separate D_1 and D_2 agonists, we tested co-activating D_1 and D_2-like receptors with the D_1/D_2 co-agonist SKF 83959 (50 μM) (Rashid et al., 2006; Thompson et al., 2016). As predicted, the co-agonist elicited a more robust depolarization of the ventral root DC potential, compared with the D_1 agonist, when applied alone (Fig. 4A, Ci; D1, $n = 8$; D_1/D_2, $n = 8$; one-way ANOVA, $F_{(2,21)} = 5.2$, $p = 0.01$; Tukey post hoc, $p = 0.03$). Interestingly, the co-agonist also robustly facilitated superimposed spontaneous activity, as indicated by a larger response ratio than co-application of the D_1 and D_2 agonists produced (Fig. 4B, Cii; one-way ANOVA, $F_{(3,29)} = 12.0$, $p < 0.001$; Tukey post hoc, $p = 0.004$). These data suggest that under certain conditions, D_2 receptors that are typically inhibitory can play an excitatory role via D_1/D_2 co-activation, and contribute to lumbar motor network excitation in the neonatal mouse spinal cord.

Low levels of endogenous spinal dopamine inhibit spontaneous activity

We next examined the contribution of the endogenous dopamine system to perinatal spinal network function. Endogenous levels of dopamine were increased by blocking the dopamine transporter (DAT) with an antagonist GBR 12909 (10 μM). Blocking DAT ($n = 8$ preparations) produced a modest but significant reduction in spontaneous activity compared to time-matched vehicle controls, reflected by a

reduced response ratio (Fig. 5A, Bi; one-way ANOVA, $F_{(2,19)} = 18.0$, $p < 0.001$) and a reduced number of spontaneous episodes (Fig. 5Bii; n = 8, two-way ANOVA, $F_{(2,20)} = 11.8$, $p = 0.0004$), with no change in amplitude (Fig. 5Biii; n = 6, two-way ANOVA, $F_{(2,20)} = 1.3$, $p = 0.3$). We questioned whether extracellular dopamine metabolism may have dampened the effect of the reuptake blocker, thus diminishing the predicted increase in endogenous dopamine levels. Therefore, we repeated this experiment in the presence of bifemelane, a monoamine oxidase A & B inhibitor. Under these conditions, we found further reductions in spontaneous activity when DAT was blocked, as indicated by a significantly reduced response ratio **(**Fig. 5Bi; n = 6, one-way ANOVA, $F_{(2,19)} = 18.0$, $p < 0.001$). Burst analysis revealed significantly fewer episodes (Fig. 5Bii; n = 6, two-way ANOVA, $F_{(2,20)} = 11.8$, $p = 0.0004$) with no change in amplitude (Fig. 5Biii; n = 6, two-way ANOVA, $F_{(2,20)} = 1.3$, $p = 0.3$).

We followed these experiments up with high-performance liquid chromatography (HPLC) to verify endogenous levels of dopamine. In P3 lumbar spinal cords (n = 11) we detected low levels of dopamine; in P60 adults (n = 17) we detected a threefold increase in dopamine levels (Fig. 5Biv; Mann–Whitney U = 10.0, T = 76, $p < 0.001$). Thus, our in vitro experiments indicated that low levels of endogenous dopamine play a role in D_2-mediated inhibition.

D_1 receptor activation increases motoneuron excitability by reducing afterhyperpolarization properties

In the next set of experiments, we were interested in determining the cellular mechanisms that mediate dopamine's complex modulatory effects on spinal network output. As integrators of premotor network activity that generate many of the rhythmic outputs of the spinal cord, motoneurons are ideally suited to amplify spontaneous activity and respond to dopaminergic modulation. Given that they not only serve as the final output for spinal networks, but they also participate in the generation of rhythmic activity (Falgairolle et al., 2017), we initially selected motoneurons as a locus for determining the cellular mechanisms for dopaminergic excitation and inhibition. We made whole-cell patch-clamp recordings

from 75 motoneurons (across 42 animals). Some of these motoneurons (n = 18 across seven animals) were filled with fluorescein-conjugated dextran amine (FITC; Molecular Probes, Inc., Eugene Oregon) and verified post hoc using immunohistochemistry for the presence of choline acetyltransferase (ChAT; Fig. 6A). One hundred percent of filled cells were ChAT positive indicating that we were indeed recording from motoneurons. Electrical properties measured in a group of these cells (n = 8 cells across five animals) were comparable to cells from putative motoneurons recorded in the remaining experiments (Table 1) indicating that these cells are also likely motoneurons. Motoneurons also display characteristic time-dependent changes in repetitive firing frequency during sustained depolarizing current injections (Fig. 6 Cii) (Miles et al., 2005; Button et al., 2007; Bos et al., 2018). We found that all but two cells demonstrated a time-dependent reduction in firing rate throughout the duration of a 0.5 s depolarizing current injection, as indicated by the ratio between maximum steady-state and first spike interval frequencies. This phenomenon is known as spike frequency adaptation (SFA; mean SFA ratio = 0.47 ± 0.19). In addition, doublet firing occurred at the onset of repetitive firing in 5 cells (8%).

Consistent with previous reports from our laboratory (Han et al., 2007a; Han and Whelan, 2009) and with our network recordings in this report, 100 μM of dopamine increased motoneuron excitability (n = 5 cells across four animals); we reproduced this effect with the D_1 agonist SKF 81297 (20 μM; n = 8 cells across five animals). Both 100 μM dopamine and the D_1 agonist depolarized the membrane potential (Fig. 6Bi; $H_{(2)} = 18.9$, $p < 0.001$), increased negative holding current (vehicle, −7.1 ± 33 pA; DA, −247 ± 78 pA; D_1, −174 ± 49 pA; $H_{(2)} = 18.9$, $p = 0.001$) and input resistance (Fig. 6Bii; $H_{(2)} = 16.0$, $p < 0.001$), and decreased rheobase (Fig. 6Bii; $F_{(2,22)} = 5.0$, $p = 0.016$) beyond that of the time-matched vehicle control. We found no change in spike rise time ($F_{(2,22)} = 1.0$, $p = 0.4$) or half width ($F_{(2,22)} = 0.8$, $p = 0.5$). The D_1 agonist reduced the amplitude of the afterhyperpolarization (AHP); however, 100 μM dopamine did not reduce AHP amplitude beyond that of a time-matched vehicle control (Fig 6Biv; $F_{(2,22)} = 7.7$, $p = 0.003$). Frequency–current (FI) relationships were measured for steady state and first spike interval during a series of depolarizing current pulses (Fig. 6Ci). Both 100 μM dopamine and the D_1 agonist reduced the

latency to first spike beyond that of the time-matched vehicle control (Fig. 6Cii; $F_{(2,17)} = 9.6$, $p = 0.002$). Dopamine (100 μM) and the D_1 agonist increased the slope of the exponential region of the FI relationship for the first spike interval (Fig. 6Di–Dii; $F_{(2,22)} = 8.4$, $p = 0.002$) and reduced the slope of the steady-state FI relationship (Fig. 6Diii–Div; $H_{(2)} = 9.4$, $p = 0.009$). The reduction in steady-state slope was due to a leftward shift in steady-state FI relationship (Fig. 6Diii) characterized by a reduction in the threshold for repetitive firing (Fig. 6Ciii; $H_{(2)} = 14$, $p < 0.001$) with no change in the maximum steady-state firing rate ($H_{(2)} = 1.4$, $p = 0.5$). These results indicate that activation of D_1 receptors elicit consistent effects as high concentrations of dopamine on motoneuron excitability and is a likely mechanism contributing to dopaminergic excitation of motor output.

Dopaminergic inhibition through D_2 - receptor hyperpolarization of distributed populations of ventral interneurons

We next set out to determine the cellular mechanisms that mediate the inhibitory effects of dopamine on spinal network output with motoneurons as our first target. In contrast to our network recordings, low concentrations of dopamine (1–10 μM; n = 20 cells across 14 animals; Table 1) and the D_2 agonist quinpirole (20 μM; n = 12 cells across seven animals; Table 1) did not alter any passive, spike or repetitive firing properties of motoneurons beyond that of the time-matched vehicle control (n = 12 cells across six animals). A lack of responsiveness was not due to the diversity of motoneurons as there was no correlation between cell capacitance and changes in membrane potential or holding current elicited by low concentrations of dopamine ($r = -0.3$, $p = 0.13$) or quinpirole ($r = -0.1$, $p = 0.72$). These results suggest that the inhibitory actions of dopamine on spinal network output are not due to D_2-receptor inhibition of intrinsic motoneuron excitability; instead, dopamine may be acting on premotor interneurons.

Many of the premotor interneurons that produce the rhythmic activities generated by the spinal cord are distributed across lamina's VII - X of the ventral lumbar spinal cord. We next recorded from ventral

interneurons located in lamina VII–X to determine a cellular locus for D_2-mediated inhibition of spinal network output (n = 30 cells across 17 animals; Table 2). Quinpirole produced a sustained hyperpolarization of the resting membrane potential in 33% of interneurons (Fig. 7B, C, Di; n = 10; dVm = −4.8 ± 2.4 mV; two-way ANOVA, $F_{(2,37)} = 26.1$, $p < 0.0001$) and a transient hyperpolarization of membrane potential in 10% of interneurons (n = 3; dVm = −5.16 ± 1.9 mV) that persisted for 209 ± 108 s before returning to baseline levels. The change in resting membrane potential was greater in the responders compared to non-responders (dVm responders = - 4.8 ± 2.4 mV; dVm non-responders = 1.6 ± 1.9 mV; unpaired t-test $t_{(28)} = 7.8$, $p < 0.0001$). Quinpirole reduced the input resistance (Fig. 7Dii; two-way ANOVA, $F_{(2,37)} = 4.1$, $p = 0.025$) and increased the spike rise time (Fig. 7Div; two-way ANOVA, $F_{(2,35)} = 5.2$, $p = 0.01$; Dunn post hoc test, p=0.02) but not the half width ($F_{(2,35)} = 2.6$, $p = 0.086$) in the group of responding interneurons ("responders"). For both responders and nonresponders, quinpirole did not alter rheobase (Fig. 7Diii; two-way ANOVA, $F_{(2,37)} = 0.5$, $p = 0.6$), action potential threshold (two-way ANOVA, $F_{(2,37)} = 0.3$, $p = 0.7$), AHP amplitude (two-way ANOVA, $F_{(2,37)} = 0.04$, $p = 0.96$), duration (two-way ANOVA, $F_{(2,37)} = 0.8$, $p = 0.45$), threshold for repetitive firing (two-way ANOVA, $F_{(2,37)} = 0.01$, $p = 0.98$), maximum steady-state firing rate (Fig. 7Dvi; two-way ANOVA, $F_{(3,37)} = 0.8$, $p = 0.5$) or steady-state FI slope (Fig. 7Dv: two-way ANOVA, $F_{(2,37)} = 0.9$, $p = 0.4$). The capacitance (two-way ANOVA, $F_{(2,37)} = 4.2$, $p = 0.02$) and holding current (two-way ANOVA, $F_{(2,37)} = 4.9$, $p = 0.02$) were higher in responders than in nonresponders (Table 2) and a greater proportion of responders were localized to more medial regions of spinal slices (Fig. 7B), where putative commissural interneurons reside (Quinlan and Kiehn, 2007).

We next set out to determine the type of interneurons that were hyperpolarized by quinpirole. Given that many of the responding cells were located medially, we next targeted descending commissural interneurons (dCINs; n = 10 cells across five animals; Table 2) since this population can be identified based on anatomical connectivity (Butt and Kiehn, 2003; Kiehn and Butt, 2003), display intrinsic burst properties (Abbinanti et al., 2012) and are rhythmically-active during neurochemically-evoked fictive

locomotion (Zhong et al., 2006). dCINs were retrogradely labelled with tetramethylrhodamine-conjugated dextran amine (molecular weight (MW) 3000; Molecular Probes, Inc.) inserted into the ventrolateral funiculus at the L4 segment (Fig. 7A). In contrast to our hypothesis, only one dCIN responded with a sustained hyperpolarization and two were transiently hyperpolarized (Fig. 7B) by quinpirole. Quinpirole did not alter any passive, spike, or repetitive firing properties of dCINs (n = 10; Fig. 7D). These data suggest that the dCINs, although responsive in similar proportions to our global interneuron survey, do not exclusively account for the 33% responding group and, therefore, are likely, not responsible for the observed network effects. Interestingly, when all interneuron data were pooled (n = 40 cells), irrespective of responsiveness as indicated by changes in resting membrane potential, quinpirole had the greatest effect in cells that had a higher maximum steady-state firing rate at baseline (Fig. 7DViii; $r = -0.37$, $p = 0.026$). There was no correlation between baseline FI slope and changes in FI slope in response to quinpirole ($r = -0.09$, $p = 0.6$).

While dCINs can be identified anatomically, they are heterogeneous with respect to their neurotransmitter phenotype (Restrepo et al., 2009) and as a result have varying contributions to network activities (Butt et al., 2002; Zhong et al., 2006; Quinlan and Kiehn, 2007). We therefore next targeted V3 interneurons which are exclusively glutamatergic, contribute to the stabilization of locomotor-like rhythmicity and can be identified genetically based on the expression of the Sim1 transcription factor (Zhang et al., 2008). Heterogeneity with respect to location, morphology and electrophysiological properties has also been reported in V3 interneurons (Borowska et al., 2013, 2015) which may be accounted for in part by a recently described hierarchical microcircuit whereby a medial population projects to a lateral population which provide glutamatergic excitation of ipsilateral motoneurons. Both populations also project commissurally and receive recurrent glutamatergic inputs from intra and intersegmental ipsilateral motoneurons (Chopek et al., 2018). Given that dopamine inhibits ventral root-evoked locomotor activity, which may be mediated by this circuit (Falgairolle and O'Donovan, 2019), through D_2-receptor signalling

(Humphreys and Whelan, 2012), we hypothesized that V3 interneurons may be a cellular locus for D_2-mediated inhibition of spinal network activity.

Consistent with our global interneuron survey, quinpirole produced a sustained hyperpolarization of the resting membrane potential in a proportion of V3 interneurons (n=5 cells; 27%) that we recorded from (total V3 interneurons n=23 cells, 7 animals) and transient hyperpolarization in 3 (13%) V3 interneurons. The magnitude of the response in the 5 cells that responded with a sustained hyperpolarization was variable and approached, but did not reach, significance (Supp Figure 1; paired t-test: $t_{(4)}= 2.5$, $p = 0.06$); however, did reach significance when the cells that responded with a transient hyperpolarization were included in the analysis (paired t-test: $t_{(6)} = 2.7$, $p = 0.03$). Consistent with our global interneuron survey the change in resting membrane potential elicited by quinpirole was significantly greater in responding (n = 5; dVm = -1.9 ± 1.9 mV) compared to non-responding (n = 15; dVm = -0.3 ± 1.0 mV) V3 interneurons (unpaired t-test: $t_{(16)} = 3.8$, $p = 0.002$).

Discussion (1500 words)

Dopamine is important for the control of rhythmically active motor circuits across phyla (for review see (Sharples et al., 2014)). The effects of dopamine on developing mammalian spinal circuits have been previously investigated during fictive locomotor activity (Barriere et al., 2004; Humphreys and Whelan, 2012; Sharples et al., 2015; Picton et al., 2017; Acton et al., 2018), but there is little evidence that mice participate in regular coordinated locomotor activity perinatally. Rather, the majority of the time they show ataxic bouts of movement with occasional periods of coordinated activity. Our work demonstrates that when spontaneous activity is expressed and excitability is low, the modulatory effects of dopamine are fundamentally different. Under these conditions, dopamine acts primarily as a network excitability brake, since the low endogenous levels in the spinal cord postnatally would activate high-affinity D_2-like receptors. Low levels of endogenous dopamine inhibit network output by acting in parallel on higher affinity D_2-like and α2-adrenergic receptors. The inhibitory actions of D_2 receptors are mediated in part by hyperpolarizing premotor interneurons but not motoneurons. However, the D_2 actions are not localized to particular classes of interneurons. This result is in line with the rhythm generating kernel of the locomotor central pattern generator being distributed across several classes of interneurons (Dougherty et al., 2013; Kiehn, 2016; Caldeira et al., 2017).

Excitatory mechanisms of dopaminergic modulation

Historically, investigations on the dopaminergic regulation of mammalian spinal networks have used higher concentrations of dopamine which are necessary to elicit observable effects during high excitability states such as fictive locomotion (Whelan et al., 2000a; Barriere et al., 2004; Lapointe et al., 2009; Sharples et al., 2015; Picton et al., 2017). High concentrations of dopamine increase motoneuron excitability by reducing A-Type and calcium-dependent potassium conductances that contribute to reduced afterhyperpolarization and an increased gain for repetitive firing (Han et al., 2007a). Our data validate those findings and extend them to show that D_1 receptors, but not D_2 receptors, can reproduce

these effects. Furthermore, our network data revealed that the excitatory actions of dopamine are not only due to the activation of D_1 receptors but also co-activation of D_2 receptors. D_1 and D_2 receptors become co-activated or form heterodimeric complexes that augment neuronal excitability through PLC-dependent increases in intracellular calcium (LaHoste and Marshall, 1993; Lee et al., 2004; Rashid et al., 2007; Thompson et al., 2016). Our pharmacological and immunoprecipitation data indicate that this may also occur in the neonatal mouse spinal cord. D_1 receptors have been reported to form heteromers with A_1 adenosine receptors in motoneurons (Rivera-Oliver et al., 2018); however, our whole-cell recordings do not indicate that D_2 receptors regulate motoneuron excitability. Therefore, excitatory D_1/D_2 interactions may not occur in motoneurons. D_2 receptors seem to preferentially alter episode frequency, and not amplitude or motoneuron excitability, making the premotor network a likely locus of D_1 and D_2 receptor co-activation and may occur in presynaptic contacts of premotor–motoneuron synapses, similar to observations in the striatum (Perreault et al., 2010).

Inhibitory mechanisms of dopaminergic modulation

Although the excitatory D_1 system is functional, given the low levels of endogenous dopamine present in the spinal cord, it is more likely that dopamine's primary role in the control of neonatal spinal networks is inhibitory. Consistent with our findings, others have found evidence of inhibitory dopaminergic effects on spontaneous locomotor network activities in *Xenopus* (Clemens et al., 2012; Picton and Sillar, 2016), larval zebrafish (Thirumalai and Cline, 2008), lamprey (McPherson and Kemnitz, 1994; Kemnitz et al., 1995; Svensson et al., 2003; Wang et al., 2011), and on reflex circuits in rodent spinal cords (Clemens and Hochman, 2004; Kawamoto et al., 2012).

The inhibitory effect of low concentrations of dopamine is mediated via parallel activation of D_2 , D_3, D_4 and α_2-adrenergic receptors, to control variables related to the network output frequency, but not amplitude. Our previous studies of locomotor-like activity implicating D_2 receptors in the control of

rhythm frequency support this notion (Humphreys and Whelan, 2012; Kawamoto et al., 2012; Sharples et al., 2015). Recent work has demonstrated that dopamine increases the activity of the inhibitory sodium-potassium ATPase pump in motoneurons (Picton et al., 2017), which was considered as a potential locus for D_2 regulation of locomotor rhythm frequency and stability (Sharples, 2017); however, the population of motoneurons studied here do not appear responsive to D_2 agonists or low concentrations of dopamine.

Our data suggest that D_2 receptors regulate network output by hyperpolarizing a proportion of ventral interneurons. Based on our responsiveness criteria, a majority of cells that responded to a D_2 agonist with sustained hyperpolarization of the membrane potential were localized more medially in lumbar slices. We tested the hypothesis that a subpopulation of interneurons was D_2 sensitive, and tested both dCINs and genetically identified V3 interneurons. Our hypothesis was not supported, and similar proportions of D_2 sensitive neurons were found. To our knowledge, there are limited investigations that examine modulation of genetically-defined interneurons that compose spinal motor networks (Dietz et al., 2012; Husch et al., 2012, 2015). This is important because neuromodulators shape network output, and as a result change behaviour, by altering intrinsic and synaptic properties of the elements that compose the network (Marder, 2012). Our data suggest that there is heterogeneity in the responsiveness to neuromodulators within a class of genetically defined interneurons and that D_2 actions may not be localized to a particular class of interneurons. One possibility is that neuromodulators elicit a robust effect on network output through distributed control across multiple classes of genetically-defined interneurons which would be consistent with findings that the kernel of the CPG is also distributed across several classes of interneurons (Dougherty et al., 2013; Kiehn, 2016; Caldeira et al., 2017). Another possibility is that D_1-like and D_2-like receptors are spatially patterned such as in the superior colliculus where they are segregated into distinct functional zones (Bolton et al., 2015).

Developmental considerations for the endogenous dopaminergic system

During perinatal development, chloride-mediated synaptic transmission still causes partial depolarization (Jean-Xavier et al., 2007). An inhibitory brake would prevent runaway excitation of spinal network activity during this critical period of development. A robust background inhibitory system mediated by the parallel inhibitory action of D_2, D_3, D_4, and α2-adrenergic receptors activated by low levels of endogenous dopamine would counteract depolarizing chloride-mediated transmission.

Similar to previous reports (Milan et al., 2014), we showed that spinal dopamine levels are low perinatally and increase threefold into adulthood. With dopaminergic fibres present only in trace amounts perinatally (Commissiong, 1983) and peaking by P21, the source of spinal dopamine during perinatal development comes into question. Some have proposed that the brain is a dopaminergic endocrine organ, acting as an extrinsic source (Ugrumov et al., 2012). Alternatively, monoamines may be produced intrinsically within the spinal cord in a multistage process. This is the case following spinal cord injury when descending inputs are compromised, and endothelial cells of the vasculature (Li et al., 2014) and classes of local interneurons change their enzymatic phenotype to become capable of synthesizing monoamines like dopamine from the precursor levodopa that can cross the blood-brain barrier (Wienecke et al., 2014; Ren et al., 2016). While similar processes have not been studied perinatally, there is evidence of both local interneurons and endothelial cells that express aromatic L-amino acid decarboxylase, but not tyrosine hydroxylase, that may contribute to monoamine and trace amine production (Gozal et al., 2014) locally within the spinal cord.

The function of D_2-like receptors extends beyond the regulation of cellular excitability. In larval zebrafish, D_4 receptors drive the maturation of spinal locomotor network organization (Reimer et al., 2013) and function (Lambert et al., 2012). Similar processes may occur perinatally in rodents, in that the preferential activation of the D_2 receptor system may favour intracellular signalling that results in network reorganization. Serotonin receptors have been found to shape network function and inhibitory synaptic

transmission during early postnatal days of rodents (Pflieger et al., 2002; GackiÃ¨re and Vinay, 2014). Dopamine could, therefore, act analogously via the D_2-system during perinatal development.

Conclusions

We have presented data highlighting that neuromodulator actions are dependent not only on their target receptors but also on the state of the network they modulate. Our experiments, performed during a low excitability state, enabled us to link the receptor and cellular mechanisms that contribute to the diverse concentration-dependent control of spinal networks in the neonatal mouse in vitro. High concentrations of dopamine boosted network excitation by acting on D_1 receptors to depolarize motoneurons via reduced AHP. High concentrations of dopamine also co-activated D_2 receptors, likely in premotor neurons. Given the low levels of endogenous dopamine present in the neonatal spinal cord, these actions may not occur in vivo during early postnatal development. Low levels of endogenous dopamine may act as a brake on network activity during this time when excitatory neurotransmission prevails (Jean-Xavier et al., 2007). This finding is reinforced by our demonstration that low levels of exogenously applied dopamine act through D_2, D_3, D_4 and α_2-adrenergic receptors in parallel, with D_2 receptors not altering motoneuron excitability, but hyperpolarizing a proportion of premotor interneurons distributed across multiple subclasses.

Methods

Ethical approval & animals

Experiments were performed on male and female neonatal (P0–P4, n = 262) and adult (P50, n = 17) C57BL/6 mice. A subset of experiments were performed on spinal cord slices obtained from neonatal (P0-4, n=7) $Sim1^{Cre/+}$; $Rosa^{floxstop26TdTom}$ which were used to visualize and record from V3 interneurons. All procedures performed were approved by the University of Calgary Health Sciences Animal Care Committee University Committee on Laboratory Animals at Dalhousie University.

Tissue preparation

We anesthetized all animals by hypothermia. Pups were decapitated and eviscerated to expose the vertebral column and rib cage. The isolated vertebrae and rib cage were transferred to a dish lined with a silicone elastomer (Sylgard; DowDuPont, Midland, MI) and perfused with room-temperature (21 - 23ºC) carbogenated (95% O_2 / 5% CO_2) aCSF (in mM, 4 KCl, 128 NaCl, 1 $MgSO_4$, 1.5 $CaCl_2$, 0.5 Na_2HPO_4, 21 $NaHCO_3$, 30 D-glucose; 310–315 mOsm.). We exposed the spinal cord with a ventral laminectomy and isolated it by cutting the nerve roots that connected it to the vertebral column. The isolated spinal cord was then transferred to a recording chamber, perfused with carbogenated aCSF, and placed ventral side up. The bath temperature was gradually increased to 27°C (Whelan et al., 2000b). We let the spinal cords stabilize for 1 hour before performing experiments.

Spinal cord slice preparation

Following isolation, spinal cords were transected above the tenth thoracic (T10) and below the first sacral (S1) segments and transferred to a slicing chamber. Pre-warmed liquefied 20% gelatin was used to secure cords to an agar (3%) block that was super-glued to the base of a cutting chamber and immersed in ice-cold, carbogenated, high-sucrose slicing aCSF (in mM, 25 NaCl, 188 sucrose, 1.9 KCl, 10 Mg SO_4, 1.2 Na_2HPO_4, 26 $NaHCO_3$; 25 D-Glucose; 340 mOsm). Using a vibratome (Leica, Bussloch, Germany) we cut 250-µm-thick lumbar slices, collected and transferred them to a recovery chamber containing regular carbogenated aCSF (see Tissue Preparation) heated to 32ºC for one hour, then maintained them at room temperature for at least 30 minutes before transferring them to a recording chamber.

Labelling of descending commissural interneurons (dCINs)

We retrogradely labelled dCINs by inserting tetramethylrhodamine-conjugated dextran amine crystals (MW 3000; Molecular Probes, Inc.) into a cut in the ventrolateral funiculus at the L4 segment. Spinal

cords recovered for 4 hours to allow retrograde uptake of the fluorescent dye. Fluorescently-labelled cells were visualized with epifluorescent illumination.

Electrophysiological recordings

Extracellular neurograms were recorded by drawing ventral roots of the second (L2) and fifth (L5) lumbar segments into tight-fitting suction electrodes fashioned from polyethylene tubing (PE50). Signals were amplified 1000× in total via 10× pre-amplification and 100× second-stage amplification (Cornerstone EX4-400 Quad Differential Amplifier; Dagan Corporation, Minneapolis, MN). Amplified signals were band-pass filtered (0.1–1000 Hz) and digitized at 2.5 kHz (Digidata 1440A/1550B; Molecular Devices, Sunnyvale, CA). Data were acquired in Clampex 10.4/10.7 software (Molecular Devices) and saved on a Dell computer for offline analysis. All experiments were performed on spinal cords naïve to drugs and experimental treatment.

Whole-cell patch-clamp recordings

Spinal cord slices were gently transferred to a recording chamber perfused with room-temperature carbogenated recording aCSF (in mM, 128 NaCl, 4 KCl, 1.5 $CaCl_2$, 1.0 $MgSO_4$, 0.5 Na_2HPO_4, 21 $NaHCO_3$, 30 D-glucose; approximately 310 mOsm) and stabilized in the recording dish with a stainless-steel harp. We gradually heated aCSF to 27°C. Slices were visualized (Olympus BX51WI; Olympus Corporation, Tokyo, Japan) under 5× magnification and putative motoneurons identified using a 40× objective with infrared differential interference contrast (IR-DIC) illumination. We identified putative motoneurons based on their location in the ventrolateral spinal cord and a soma diameter of greater than 20 µm. A cohort of motoneurons was passively filled with fluorescein dextran amine (FITC; MW 3000; 200µM; Molecular Probes, Inc.) added to the intracellular solution to visualize and localize the recorded cells, for 20–60 minutes and motoneuron identity was verified post hoc by performing immunohistochemistry for choline acetyltransferase (ChAT). To verify motoneuron identity in

subsequent experiments, basal biophysical properties of putative motoneurons were compared with the FITC-filled ChAT-positive cells. We identified no differences in basal biophysical properties of ChAT-positive identified cells, compared with cells in other experiments identified by position and size (Table 1). In one set of experiments, we recorded from ventral interneurons in lamina VII–X, descending commissural interneurons (dCINs) and V3 interneurons of the lumbar spinal cord (Table 2). We measured the distance of each interneuron from the central canal (LinLab2; Scientifica, Uckfield, UK) and normalized position, relative to lateral and ventral borders, and plotted the normalized positions on a template transverse spinal cord. Responsiveness was determined by the change in resting membrane potential. All experiments were performed on one cell per slice to ensure that all cells were naïve to treatment.

Recording electrodes were pulled from borosilicate capillary tubes (O.D. = 1.5mm, I.D. = 0.86 mm) using a Flaming/Brown Model P-97 micropipette puller (Sutter Instrument, Novato, CA). Pipettes pulled to record from motoneurons and interneurons were within the range of 3–5 MΩ and 6–9 MΩ, respectively. Pipettes were backfilled with intracellular solution (in mM, 130 K-gluconate, 0.1 EGTA, 10 HEPES, 7 NaCl, 0.3 $MgCl_2$, 2 ATP, 0.5 GTP, 5 phosphocreatine; 280 mOsm). Intracellular solutions were balanced to a pH of 7.3 with 10 M KOH and osmolality was cross-checked to fall within the range of 275–290 mOsm. Data were acquired at 10 kHz using Clampex software (PClamp 10.4; Molecular Devices).

We examined intrinsic properties of motoneurons and ventral interneurons and terminated experiments if access resistance was greater than 25 MΩ for motoneurons and 35 MΩ for interneurons, if cells had a resting membrane potential greater than −50 mV, or if action potential amplitude was less than 60 mV at baseline. Cells were excluded from analysis if access resistance deviated by more than 20% by the end of the recording. We held all cells at a membrane potential of approximately −75 mV during experiments, after correcting for a liquid junction potential of 14.3 mV. The liquid junction potential was calculated in Clampfit (PClamp 10.4; Molecular Devices), using the ionic composition of our extracellular and

intracellular solutions. Protocols for the examination of intrinsic properties have been described elsewhere (Nakanishi and Whelan, 2010).

Pharmacology

Dopamine hydrochloride (Sigma-Aldrich, Inc., St. Louis, MO) was bath applied in separate experiments at 1 μM, 3 μM, 10 μM, 30 μM, 100 μM, and 300 μM to determine dose-dependent effects on motor activity. The receptor-selective agonists we used included SKF 81297 for D_1-like receptors (10–50 μM; Tocris, Minneapolis, MN); quinpirole for D_2-like receptors (10–50 μM; Tocris); and the D_1/D_2 receptor co-agonist SKF 83959 (10–50 μM; Tocris). For dopamine receptor antagonists we used the D_1-like antagonist SCH-23390 (10 μM; Tocris); the D_2-like antagonists sulpiride (20 μM) and L-741,626 (12 μM); the selective D_3 receptor antagonist SB 27701A (5 μM; Tocris); the selective D_4 receptor antagonist L-745, 870 (5 μM; Tocris). We also used the α_2 adrenergic receptor antagonist, yohimbine (2–4 μM; Tocris). Endogenous dopamine levels were manipulated with the DAT inhibitor GBR-12909 (10 μM; Hello Bio, Princeton, NJ) and the monoamine oxidase A & B inhibitor bifemelane (50 μM; Tocris).

Immunoprecipitation for D_1 and D_2 receptors

Spinal cords were dissected in ice-cold (4–8ºC) aCSF and homogenized in lysis buffer containing 50 mM TrisHCl, 150 mM NaCl, 10 mM EDTA, 0.1% Triton-X, and 5% Glycerol. Lysis buffer contained protease inhibitors (Sigma) and phosphatase inhibitors (GBiosciences). We homogenized three spinal cords in 100 μL of buffer and incubated them on ice for 1 hour before centrifuging them at 10,000 rpm for 30 minutes at 4ºC. Lysates were then extracted and stored at −20ºC.

To reduce nonspecific binding, we first incubated lysates in anti-rabbit Ig agarose beads (Trueblot; Rockland Inc., Limerick, PA) for 30 minutes, on ice and in the absence of primary antibody. We then removed the supernatant and incubated the lysates on ice for 1 hour with rabbit antibody to D_2 receptors

(1 μg per 100 μL, Millipore). Anti-rabbit Ig IP beads were added and samples were incubated overnight at 4°C with gentle agitation. Immunoprecipitates were washed with lysis buffer, heated in loading buffer (350 mM Tris, 30% glycerol, 1.6% SDS, 1.2% bromophenol blue, 6% β-mercaptoethanol) to 95°C for 10 min, electrophoresed on a precast SDS gel (4–12% Tris HCl; BioRad, Hercules, CA), and transferred onto a nitrocellulose membrane. After blocking, the membranes were incubated with guinea pig antibody to D_1 receptors (1:400; Alomone, Jerusalem, Israel) and rabbit antibody to D_2 receptors (1:500; Millipore, Burlington, MA), washed, incubated for 2 hours at room temperature in fluorophore-conjugated secondary antibodies (IRDye anti-guinea pig and Trueblot anti-rabbit IgG DyLight, 1:1000), and visualized via antibody fluorescence at 680 or 800 nm (Odyssey CLx; LI-COR Biosciences, Lincoln, NE).

Post hoc verification of motoneurons

Following the completion of experimental protocols, we post-fixed slices overnight in 4% paraformaldehyde (PFA) at 4ºC, washed them the next morning in phosphate-buffered saline (PBS) for three 20-minute intervals, and stored them at 4ºC. On the day we performed immunohistochemistry, we first washed the slices for 30 minutes (3 × 10 minutes) in PBS with 0.5% Triton-X 100 (PBST) then incubated them at room temperature (21 -23ºC) for 6 hours in blocking solution containing 10% donkey serum in 0.5% PBST. Primary antibodies for choline acetyltransferase (ChAT) (1:500; goat anti-ChAT; Millipore Cat No. AB144) and the fluorescence marker (1:1000; rabbit anti-FITC, ThermoFisher Cat No. 11090) were diluted in blocking solution and the slices incubated with them for at least 24 hours at room temperature. Slices were then washed in PBST (0.5%) for 80 minutes (4 × 20 min) at room temperature before secondary antibodies (donkey anti-rabbit Alexa Fluor 1:1000, Life Technologies Cat No. A-21206; Donkey anti-Goat Alexa 568 1:1000; Cat No. A21447, Life Technologies, Carlsbad, CA) were applied for 4–8 hours at room temperature, then washed for 80 minutes in PBST (0.5%). Slices were mounted and

coverslipped with fluorescent mounting medium (Vectashield; Vector Laboratories, Burlingame, CA); coverslips were separated from slides by 500 μm spacers to prevent crushing.

Imaging

All sections processed via immunohistochemistry were imaged on a Nikon A1R MP$^+$ microscope (Nikon, Tokyo, Japan) operating in confocal mode with a 16× water-immersion objective lens (numerical aperture [NA] = 0.8, working distance [WD] = 3 mm). Image acquisition used a z-step of 1 μm and averaged two frames with a resolution of 2048 × 2048. Pixel dwell time was 2.5 ms and exposure settings were maintained for all sections. We used NIS-Elements software (Nikon) for image acquisition and ImageJ to perform maximum intensity projections of z-stacks.

High-performance liquid chromatography

Monoamine content of neonatal and adult spinal cords was measured using high-performance liquid chromatography (HPLC). We dissected spinal cords from neonatal (P3, n = 11) C57BL/6 mice in aCSF as described above and extracted adult spinal cords (P60, n = 17) with a pressure ejection method. Tissue was then flash-frozen with liquid nitrogen, stored at −80ºC, and analyzed for biogenic amines with a modified version of the Parent et al. HPLC method [76]. Tissue was homogenized in ice-cold 0.1 M perchloric acid. We centrifuged the homogenate and used 10 μl of supernatant in the assay, employing an Atlantis dC18 column (Waters, Milford, MA) and an electrochemical detector.

Data analysis

We determined the relative inhibitory or excitatory effects of dopamine and dopamine receptor agonists on spontaneous motor network activity using methods similar to those in our previous work (Sharples et al., 2015): we calculated a response ratio from single ventral root neurograms between the root mean square of 5 minutes of basal spontaneous activity and 5 minutes of activity recorded 20 minutes after

adding the drug. We subtracted 1 from the response ratio so that positive values reflect excitation and negative values reflect inhibition. The response ratio was used as a high throughput assay to detect global changes in network activity. Neurogram data were analyzed with Spike2 software. Bursts of spontaneous activity were analyzed using Clampfit (Molecular Devices) to determine how episode number and amplitude contributed to changes in response ratio. Spectral analyses were conducted using Spinalcore software (Mor and Lev-Tov, 2007) whenever we detected excitatory changes or observed rhythmicity.

Patterns of rhythmic motor activity recorded from single ventral roots were analyzed with autowavelet spectral analysis. We created and analyzed frequency–power spectrograms by selecting regions of interest around frequency ranges that coincided with those in the raw neurogram. The spectrograms revealed two high power regions that reflect distinct rhythms evoked by dopamine at high concentrations: a slow 0.01–0.04 Hz rhythm and a fast 0.8–1.2 Hz rhythm. Regions of interest were selected within these frequency ranges and analyzed over the time course of each experiment. Frequency power within selected regions of interest that corresponded to the fast and slow rhythms were used as a measure of rhythm robustness. Data were segmented into 30 s bins and averaged over 5-minute intervals for statistical analysis. We used tools available in Spinalcore for all analyses of rhythmic motor activity (Mor and Lev-Tov, 2007), consistent with Sharples and Whelan (Sharples and Whelan, 2017).

Motoneuron and interneuron intrinsic properties measured during whole-cell patch-clamp experiments were analyzed as in our previous work (Han et al., 2007b; Nakanishi and Whelan, 2010), with the exception of repetitive firing analyses, which examined the instantaneous firing rate for the first spike interval and steady-state firing separately.

Experimental design and statistical analysis

All experiments were repeated measures. We tested for differences in the magnitude of effects between conditions with one-way ANOVAs, focusing on comparisons to time-matched vehicle controls. Two-way ANOVAs compared baseline to multiple post-drug conditions. All effects surpassing a significance threshold of $p < 0.05$ were further examined with post hoc analyses. We used Holm-Sidak post hoc tests to compare all treatment conditions to the appropriate normalized time-matched vehicle control. Data that violated assumptions of normality (Shapiro–Wilk test) or equal variance (Brown–Forsythe test) were analyzed via nonparametric Mann–Whitney *U* (if two groups) or Kruskal–Wallis (if more than two groups) tests.

Table 1. Baseline motoneuron intrinsic properties.

Motoneuron basal properties (N= 65 MNs, 40 animals (P0-P4))									
Property	**Chat+ filled MNs (8,5)[1]**	**Vehicle [2] (12,6)[2]**	**1 µM DA (7,4)[3]**	**5 µM DA (7,4)[4]**	**10 µM DA (6,5)[5]**	**100 µM DA (5,4)[6]**	**SKF 81297 (8,5)[7]**	**Quinpirole (12, 7)[8]**	**(7,56) F, p**
Passive properties									
Capacitance (pF)	203±54	203±35	193±55	194.3± 45	149±66	244±54	199±50	210±43	1.6, 0.15
V_m (mV)	-73±4.1	-74±4.3	-75±4.1	-73±4.7	-73±3.7	-76±3.5	-72±6.1	-73±5.0	0.7, 0.7
$I_{Holding\ -75mV}$ (pA)	-86±148	-25±138	26±125	-63±85	23±150	-101±99	-38±87	-74±62	1.16, 0.3
Rin (MΩ)	50±15	48±24	59±44	70±83	115±84	40±9.2	71±28	49±14	2.0, 0.07
Rheobase (pA)	678±225	747±386	596±367	464±286	443±390	762±318	580±298	633±260	0.9, 0.5
Spike Properties									
AP_{TH} (mV)	-51±4.4	-55±4.4	-55±4.2	-52±5.9	-56±3.5	-53±2.5	-54±4.3	-55±4.4	1.0, 0.4
AP_{AMP} (mV)	66±5.0	71±5.9	75±6.9	76±13	76±4.2	69±5.7	71±9.6	72±6.1	1.6, 0.2
$AP_{rise\ time}$ (ms)	0.45±0.2	0.33±0.1	0.37±0.1	0.4±0.1	0.44±0.1	0.32±0.04	0.35± 0.05	0.33±0.1	1.6, 0.2
$AP_{half\ width}$ (ms)	0.59± 0.15	0.60±0.1	0.64±0.2	0.78±0.3	0.75±0.2	0.62±0.07	0.68±0.1	0.68±0.19	1.2, 0.3
$AHP_{duration}$ (ms)	73.7±29	70±18	88±34	76±13	108±38	74±16	69±23	76±26	1.5, 0.2
AHP_{AMP} (mV)	-3.9±1.1	3.6±2.2	3.1±1.4	3.2±1.4	3.4±2.1	4.7±1.2	-4.2±1.9	-4.3±1.4	0.8, 0.6
Repetitive Firing Properties									
SS F/I Slope (Hz/pA)	0.053± 0.01	0.044± 0.008	0.058± 0.008	0.052± 0.018	0.053± 0.03	0.051± 0.007	0.046± 0.008	0.053± 0.012	1.2, 0.3
Repetitive firing TH (pA)	605±446	498±254	410±271	354±200	338±327	515±253	367±186	494±173	0.8, 0.6
Max SS firing rate (Hz)	59±8.1	59±8.3	51±13	46±7.9	52±8.9	55±12	57±9.5	58±12	1.9, 0.09
First spike latency (ms)	146±86	116±57	124±77	91±34	113±79	136±55	132±67	142±50	0.5, 0.8

Table 1: Motoneuron biophysical properties at baseline. Passive, spike and repetitive firing properties of motoneurons were not different at baseline for all experimental paradigms employed in this series of experiments. Motoneuron identity was verified in a subset of experiments where cells were filled with fluorescein and post-hoc verified for choline acetyltransferase (Chat). 100% of cells were $Chat^+$ indicating that these are indeed motoneurons. Data are reported as mean ± SD. F and p values are reported from one-way analysis of variance (ANOVA).

Table 2: Interneuron biophysical properties at baseline

Ventral Interneurons (n=40 cells, 22 animals)				
Property	**Non-responders[1] (n=20,8)**	**Responders[2] (n=10,9)**	**dCINs[3] (n=10,5)**	**(2,37) F, p**
Passive Properties				
Capacitance (pF)	47±15[2]	73±40[1]	46±17[2]	4.2, 0.02
V_m (mV)	-66±4.3	-66±5.2	-66±6.0	0.02, 0.98
$I_{Holding\ -75mV}$ (pA)	-10.8±16[2]	-57±52[1]	-26±18	4.9, 0.02
Rin (MΩ)	759±466	497±248	719±326	1.6, 0.1
Rheobase (pA)	84±103	59±13	47±13	0.9, 0.4
Spike Properties				
AP_{TH} (mV)	-55±4.6	-55±2.9	-56±2.3	0.2, 0.8
AP_{AMP} (mV)	71±9.3	71±8.2	72±7.3	0.05, 0.95
$AP_{rise\ time}$ (ms)	0.99±0.48[3]	0.92±0.3[3]	1.4±0.25[1,2]	4.2, 0.023
$AP_{half\ width}$ (ms)	1.2±0.5	1.4±0.6[3]	1.9±0.4[2]	6.2, 0.005
$AHP_{duration}$ (ms)	173±96	193±76	172±81	0.2, 0.8
AHP_{AMP} (mV)	-4.9±2.7	-4.8±2.1	-4.8±2.7	0.02, 0.98
Repetitive Firing Properties				
SS F/I slope (Hz/pA)	0.24±0.07	0.21±0.09	0.2±0.1	1.0, 0.4
Repetitive firing TH (pA)	26±14	31±12	28±13	0.5, 0.6
Max firing rate (Hz)	43±16.3	39±11.6	32±5.9	2.1, 0.13
Fist spike latency (ms)	143±81	146±95	117±87	0.45, 0.6

Table 2: Interneuron biophysical properties at baseline. Passive, spike, and repetitive firing properties of ventral interneurons that responded to quinpirole with sustained hyperpolarization of membrane potential (responders) were compared with those that did not respond (nonresponders) and also descending commissural interneurons (dCINs) that were retrogradely labeled. Responders had higher capacitance and holding current than nonresponders and dCINs. Data are means ± SD; F and p values are reported from one-way ANOVAs for each property. Superscript numbers reflect significant differences between respective conditions from post hoc analysis.

Figure Captions

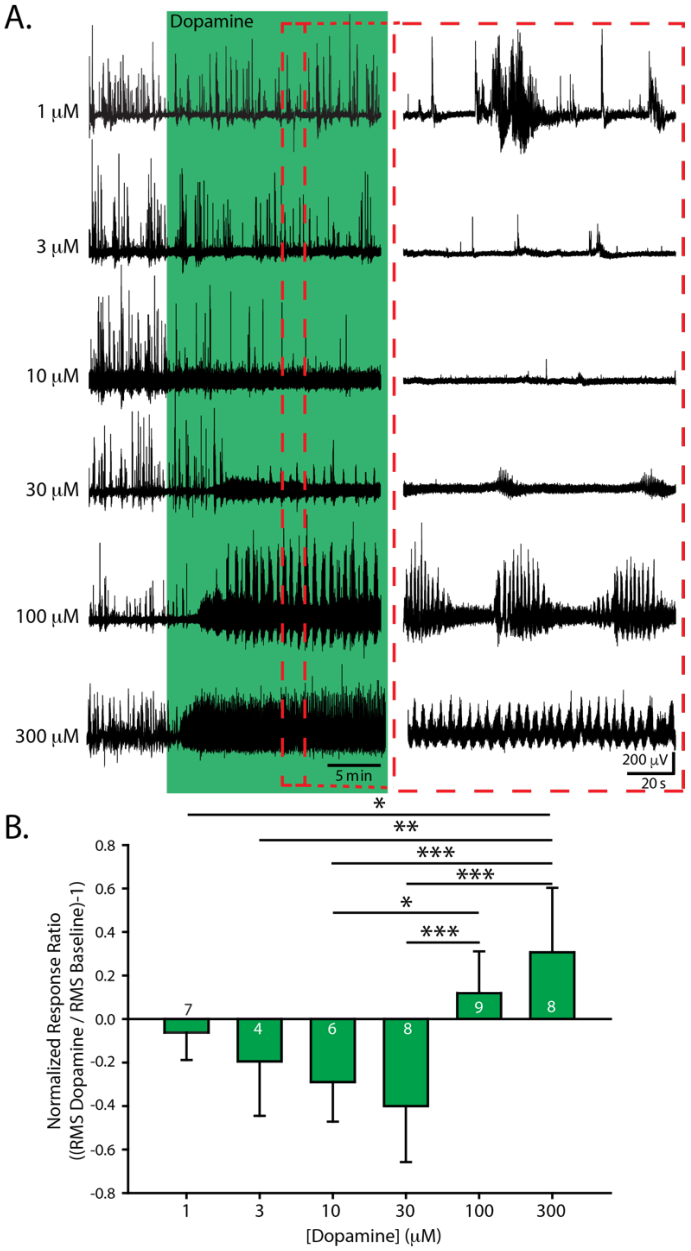

Figure 1: Dopamine evokes bidirectional dose-dependent modulation of lumbar network activity
A. Extracellular neurograms recorded from naïve single lumbar ventral root preparations after applying dopamine in various concentrations. Each row indicates a separate trial. Each recording began with spontaneous motor activity; the green section shows the effect of dopamine for each dose. The red-dashed box highlights expanded sections of data to the right of each neurogram. B. Mean normalized response ratios calculated from the root mean square of the raw neurogram during a 5-minute window, 20 minutes after dopamine application, compared to baseline activity The negative response ratios represent inhibition and positive values represent excitation. The number in each green bar indicates the number of preparations in the average for each concentration. Error bars indicate standard deviation. Asterisks denote the significance level of Tukey post hoc tests between ratio concentrations (*$p < 0.05$, **$p < 0.01$, ***$p < 0.001$).

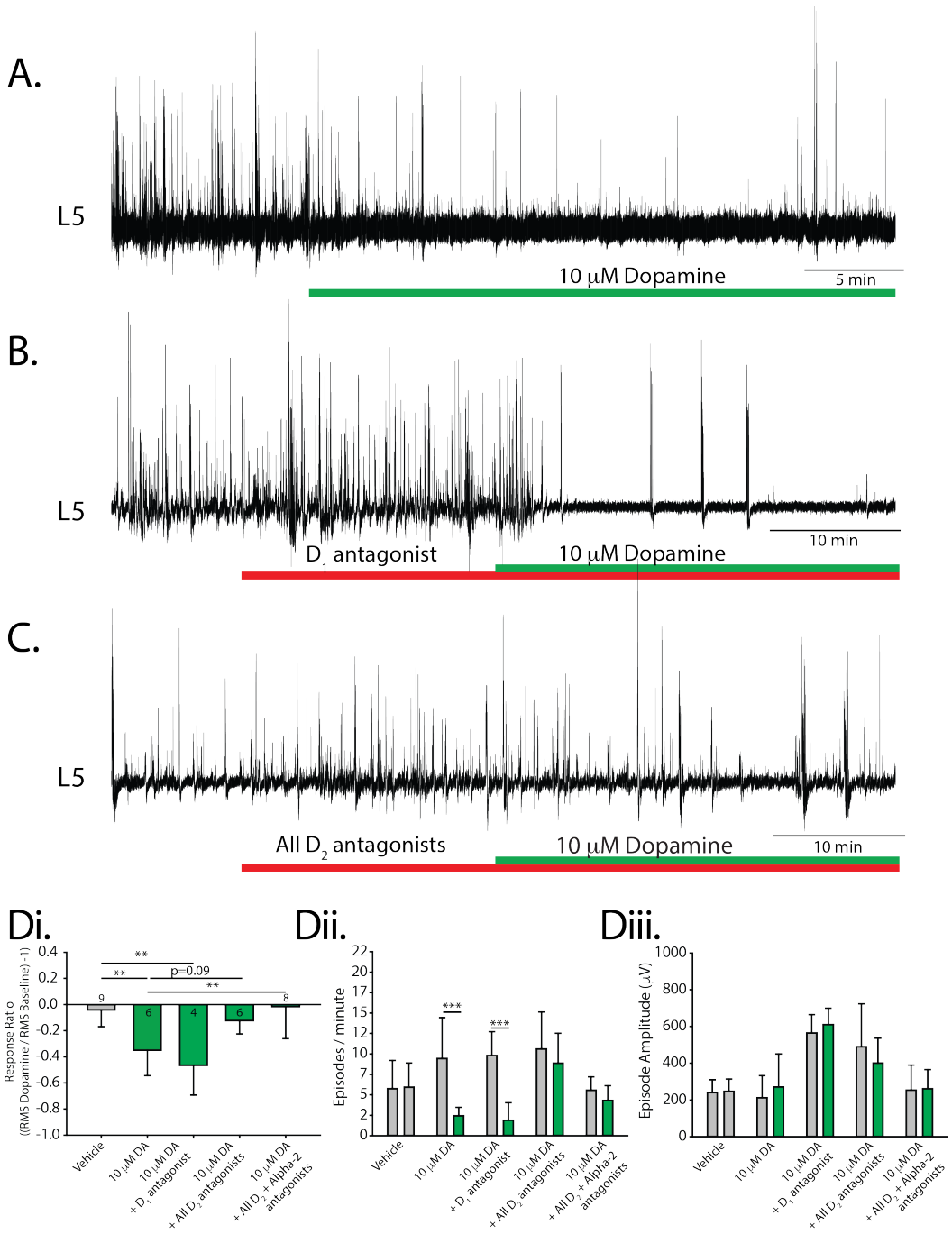

Figure 2: Receptor mechanisms for dopaminergic inhibition of spontaneous network activity.
A–C. Single ventral root (L5) extracellular neurograms of spontaneous activity in the presence of dopamine (A), a D_1 antagonist and dopamine (B), and with a cocktail of D_2 antagonists and dopamine (C). Spinal cords were perfused with receptor-preferring antagonists (red bars) 20 minutes prior to the application of low concentrations of dopamine (10 μM). D. Response ratio represents the root mean square of raw neurograms during a 5-minute window, 20 minutes after dopamine application, compared with prior to dopamine application. Negative response ratios indicate inhibition and positive values indicate excitation. The number in each bar indicates the number of preparations included in that condition's mean. Bars indicate the mean (± SD), number of episodes per minute (Dii), and amplitude (Diii) of spontaneous episodes recorded within the 5-minute epochs during which response ratios were calculated. Asterisks indicate the significance level of post hoc comparisons (*$p < 0.05$, **$p < 0.01$, ***$p < 0.001$).

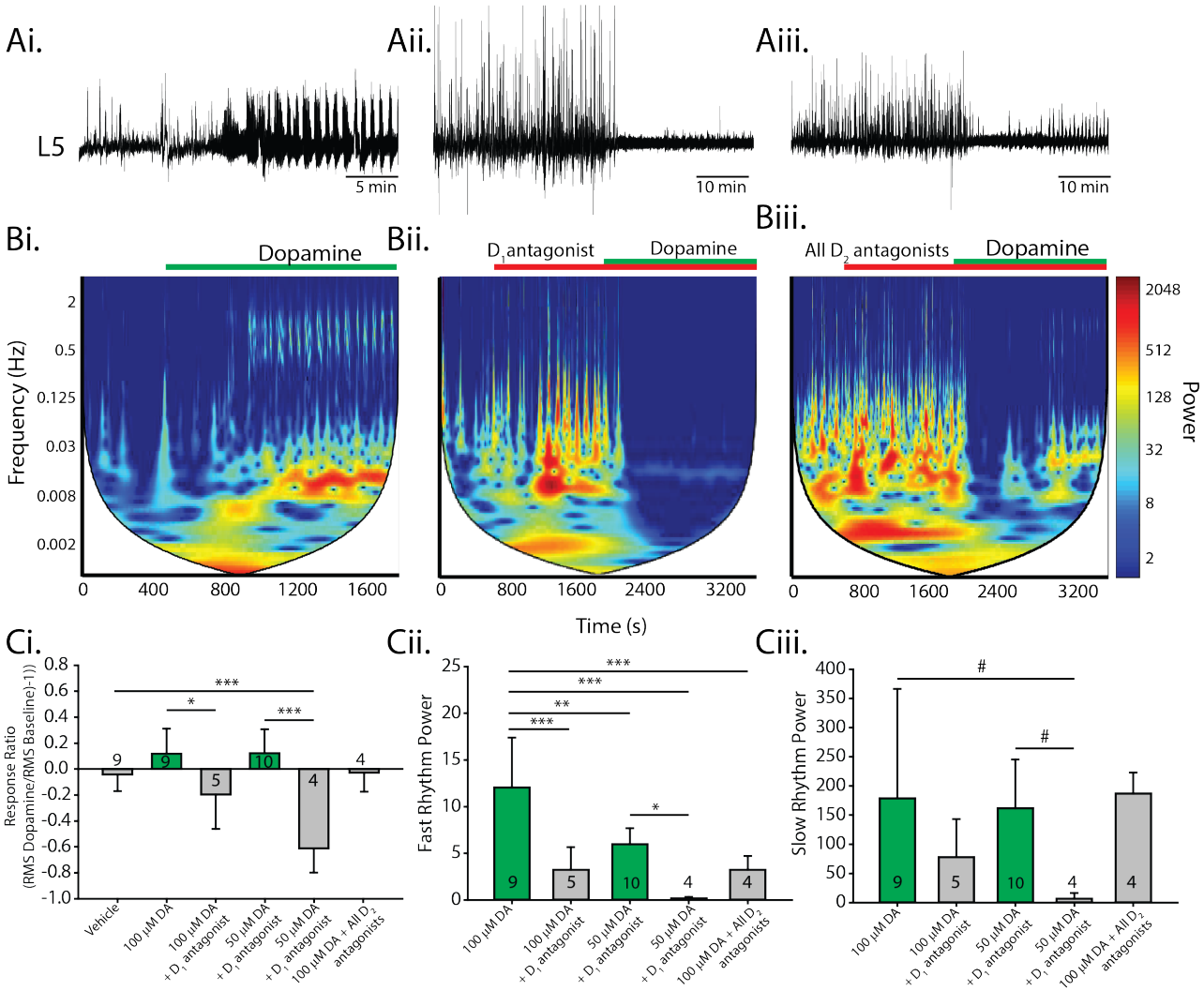

Figure 3: Receptor mechanisms for dopaminergic excitation of spinal network activity.
High concentrations of dopamine excite spinal networks and produce episodic and continuous rhythmic patterns of activity. A. Single ventral root extracellular neurograms of spinal network activity from each condition: dopamine applied alone (Ai), in the presence of a D_1 antagonist (Aii), and with a cocktail of D_2 antagonists (Aiii). Horizontal bars indicate the timing of dopamine application (green bars) and the application of receptor-preferring antagonists (red bars). B. Spectrograms show autowavelet frequency power across time, evoked at high concentrations of dopamine (50-100 µM). The colour bar indicates power magnitude, from high (warm) to low (cool colours). We selected regions of interest around regions that coincided with fast and slow rhythm frequency rhythms. Spinal cords were perfused with antagonists for 20 minutes prior to the application of dopamine. Ci. Mean response ratios (± SD), as in Fig. 2, for each condition. Spectral analysis of fast rhythm (Cii) and slow rhythm (Ciii) power following drug application for each experimental condition. Histograms present mean values ± SD, with asterisks denoting significance level of post hoc tests (*$p < 0.05$, **$p < 0.01$, ***$p < 0.001$) following one-way ANOVA (fast rhythm; Cii) or nonparametric one-way ANOVA (slow rhythm; Ciii).

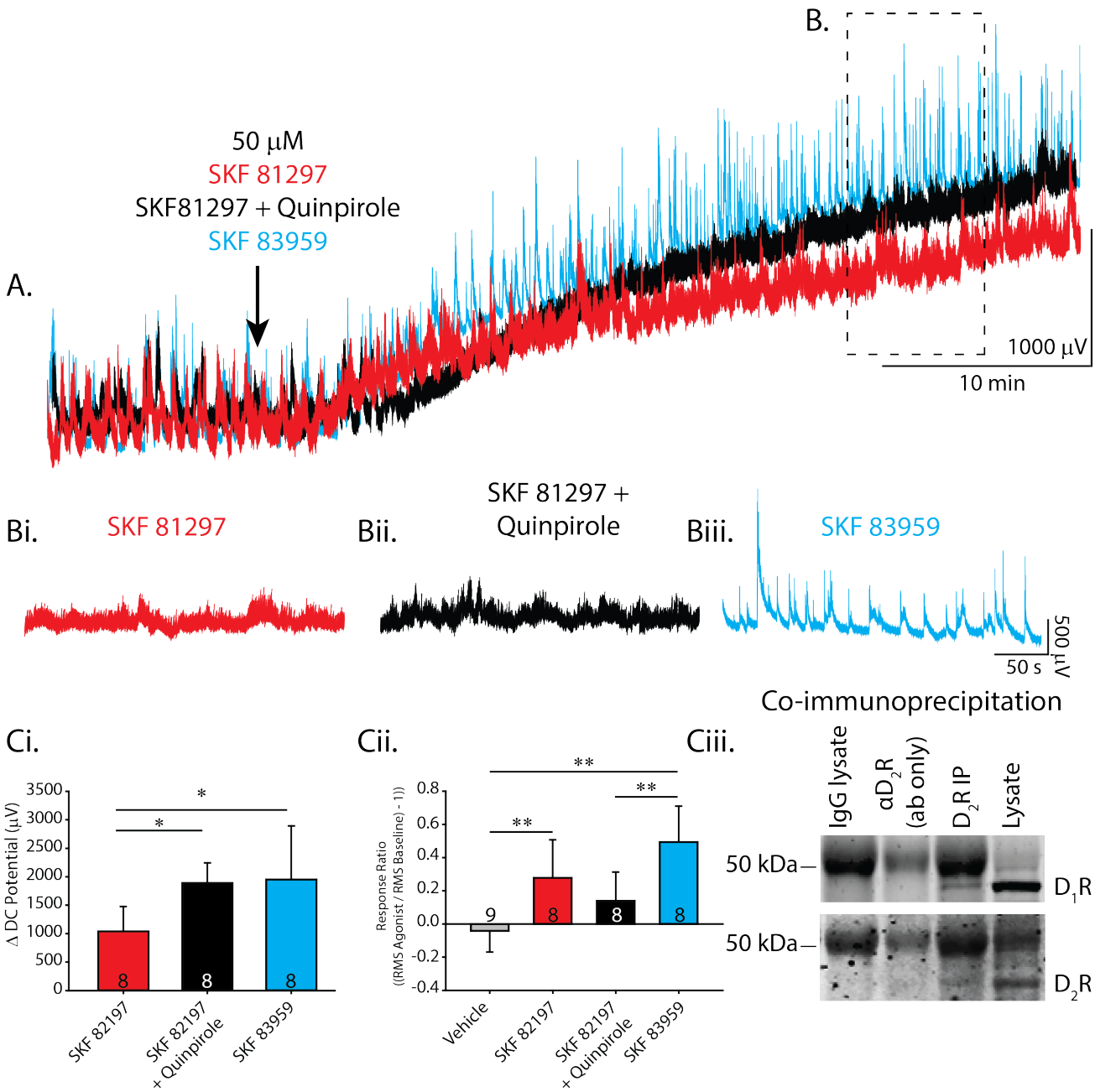

Figure 4: D_1 D_2 receptor co-activation contributes to the excitatory effect of dopamine.
A. Single ventral root extracellular DC neurograms of spontaneous activity from conditions where a D_1 agonist (SKF 81297) was applied alone (red), co-applied with a D_2 agonist (SKF 81297 + Quinpirole; black), or D_1 and D_2 receptors were coactivated by a D_1/D_2 co-agonist (SKF 83959; blue). Bi-iii. For each agonist, (B) expands the region of spontaneous activity 20–25 minutes after agonist application, as outlined by the dashed line in (A). C. Ci depicts depolarization of DC potentials from DC neurograms, averaged across the number of preparations denoted by numbers in each condition's bar. Cii shows the response ratio for each condition (as in previous figures), which represents changes in the amount of spontaneous activity. Ciii. Co-immunoprecipitation of D_1 with D_2 receptors suggests that they may interact in the neonatal spinal cord. Histograms present mean values ± SD, with asterisks denoting significance level of post hoc comparisons (*$p < 0.05$, **$p < 0.01$, ***$p < 0.001$) following one-way ANOVA.

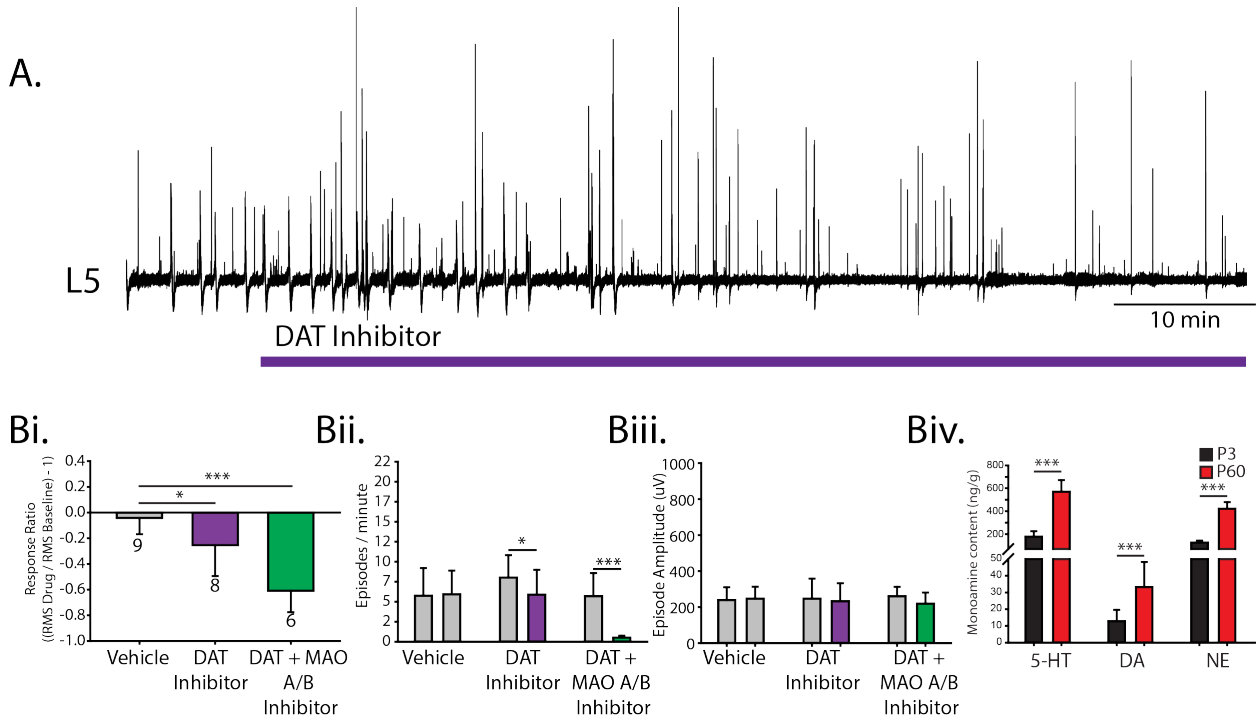

Figure 5: Inhibitory actions of endogenous dopamine in the neonatal mouse spinal cord.
A. Single ventral root (L5) neurogram of spontaneous activity after blocking the dopamine transporter (DAT) with the DAT antagonist GBR 12909 (purple) to increase the endogenous dopamine level. Dopamine reuptake was also blocked in the presence of monoamine oxidase A & B inhibitor bifemelane (green) to reduce dopamine metabolism. Bi illustrates the response ratio; negative and positive values indicate inhibition and excitation, respectively. The number below each bar represents the number of preparations for each experiment. Spontaneous episode occurrences per minute (Bii) and amplitude (Biii) were measured within the epochs where the response ratio was calculated. Histograms present mean values ± SD and asterisks indicate a significance level of post hoc analyses (*$p < 0.05$, **$p < 0.01$, ***$p < 0.001$) following one-way ANOVA for response ratios, and two-way ANOVA for burst occurrences and amplitude that compared between conditions. Biv. Endogenous levels of serotonin (5-HT), dopamine (DA) and norepinephrine (NE) were measured in neonatal (P3) and adult (P60) lumbar spinal cords with high-performance liquid chromatography.

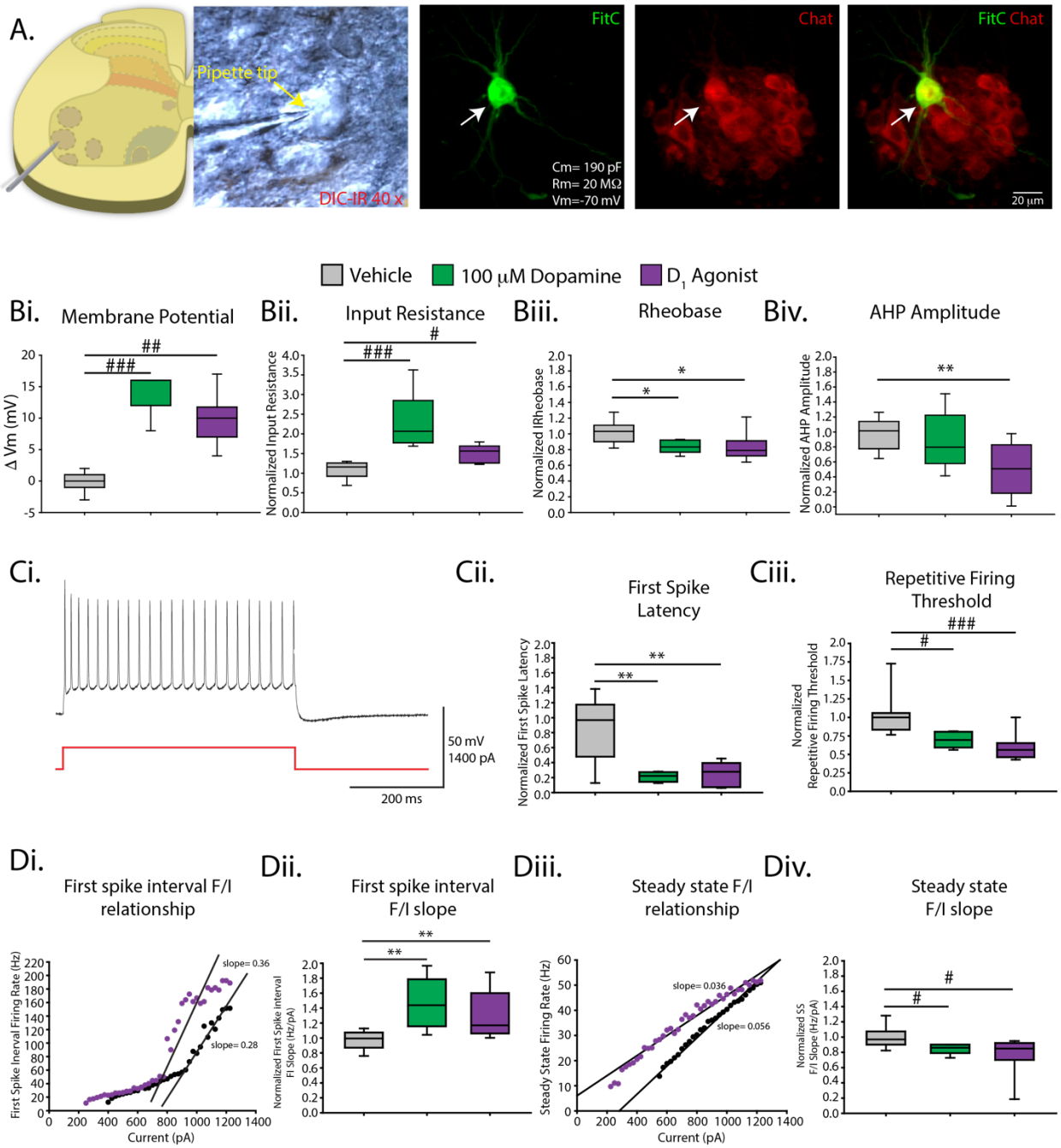

Figure 6: High concentrations of dopamine and D_1 agonists increase motoneuron excitability and reduce AHP properties.

A. Whole-cell patch-clamp recordings were obtained from motoneurons visualized with infrared differential interference contrast (IR-DIC) in lumbar slices of neonatal (P0–P4) mice. A subset of cells were filled with fluorescein (FITC, green) and verified post hoc with immunohistochemistry for choline acetyltransferase (ChAT, red). B–D. High concentrations of dopamine (100 µM, green) and the D_1 agonist SKF 81297 (20 µM, purple) increased motoneuron excitability by modulating various passive, spike, and repetitive firing properties. All measures were compared to that of time-matched vehicle control (grey). Di, Diii display representative frequency–current (FI) plots from a single cell before (black dots) and after (purple dots) application of the D_1 agonist. Box and whisker plots display interquartile range (boxes), median (horizontal black lines), max, and minimum value in data range (whiskers). Asterisks denote significance level of post hoc tests (*$p < 0.05$, **$p < 0.01$, ***$p < 0.001$) following one-way ANOVA.

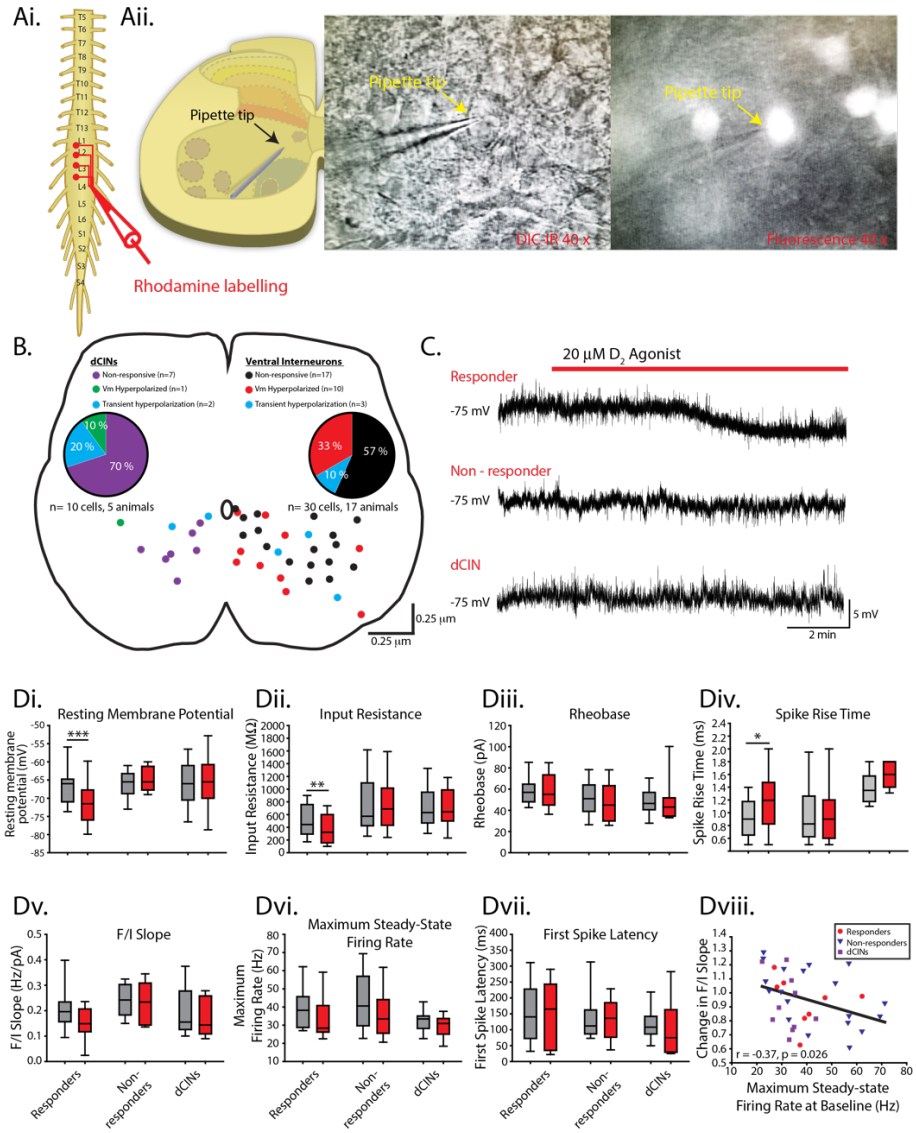

Figure 7: D_2 agonists hyperpolarize a proportion of ventral interneurons.
Whole-cell recordings obtained from lamina VII–X interneurons. Ai. Descending commissural interneurons (dCINs) were retrogradely labelled with rhodamine-conjugated dextran amine crystals inserted into the ventrolateral funiculus at L4 level. Aii. Cells were visualized in transverse lumbar slices under infrared differential interference contrast (IR-DIC) or epifluorescent illumination. B. Ventral interneuron location was measured relative to the central canal and X-Y positions normalized to the distance of ventral and lateral borders of lumbar slices. C. Whole-cell current-clamp recordings depict responsiveness of interneuron resting membrane potential to the D_2 agonist (quinpirole, 20 µM) in responders, nonresponders, and dCINs. A proportion of ventral interneurons responded to quinpirole with either a sustained (B, red and green dots) or transient (B, blue dots) hyperpolarization of the membrane potential. A reduction in input resistance and increase in spike rise time accompanied hyperpolarization in sustained responders (Dii, Div). Box and whisker plots display interquartile range (boxes), median (horizontal black lines), max, and minimum value in data range (whiskers). asterisks denote significance level from post hoc tests (*$p < 0.05$, **$p < 0.01$, ***$p < 0.001$) following two-way ANOVA. Dviii. Reductions in steady-state frequency-current (FI) slope of all cells following application of quinpirole was greatest in cells that had a higher maximum steady-state firing rate at baseline.

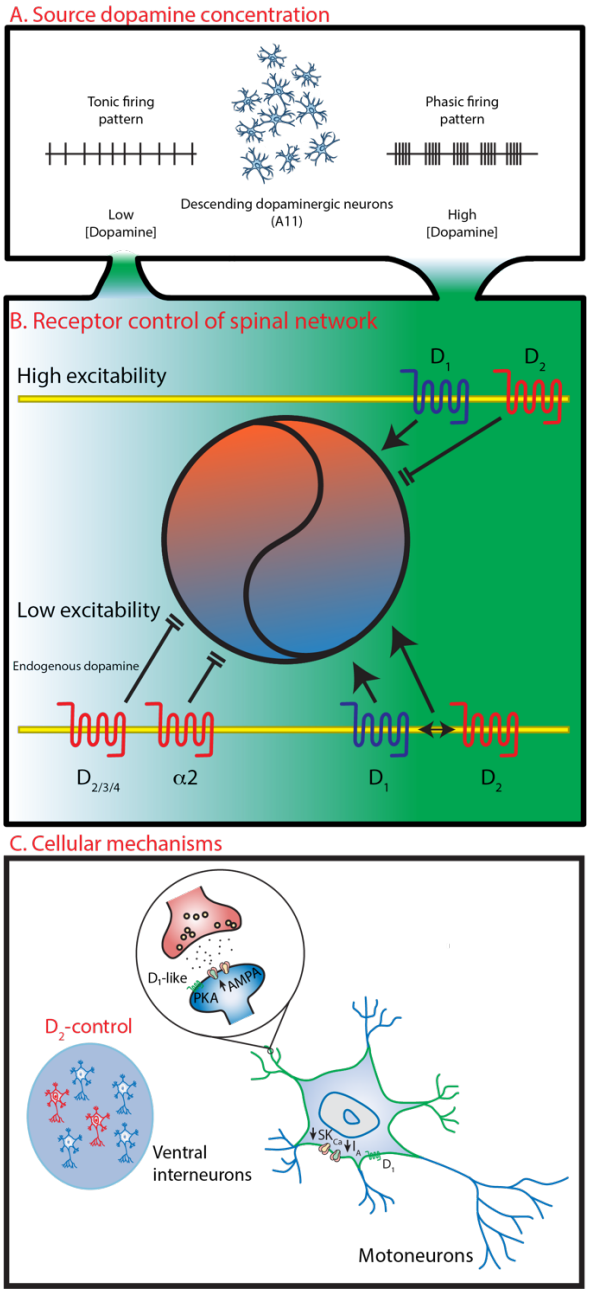

Figure 8: Dopamine exerts state and receptor-dependent control of spinal motor networks.
A. Previous work has demonstrated that tonic and phasic firing patterns of dopamine cells lead to the release of low and high concentrations of dopamine, respectively (Dreyer et al., 2010). B. During a low excitability state (blue part of the circle), low concentrations of dopamine (denoted by the green gradient) acted on D_2, D_3, D_4 and α2-adrenergic receptors in parallel to inhibit (parallel stop lines) spinal motor output. As dopamine levels rise, activation of D_1 and co-activation of D_2 receptors increase (arrowheads) spinal network output. During a high excitability state (orange part of the circle), the actions of low dopamine are not apparent and at higher concentrations, activation of D_1 receptors boost spinal network output and activation of D_2 receptors slows rhythmic activity (Sharples and Whelan, 2017). C. Higher concentrations of dopamine act through D_1 receptors to increase motoneuron excitability by reducing A-type and SKCa-dependent calcium conductance. D_2-mediated inhibition of spinal network output is triggered by reduced excitability in a proportion of ventral interneurons (red cells).

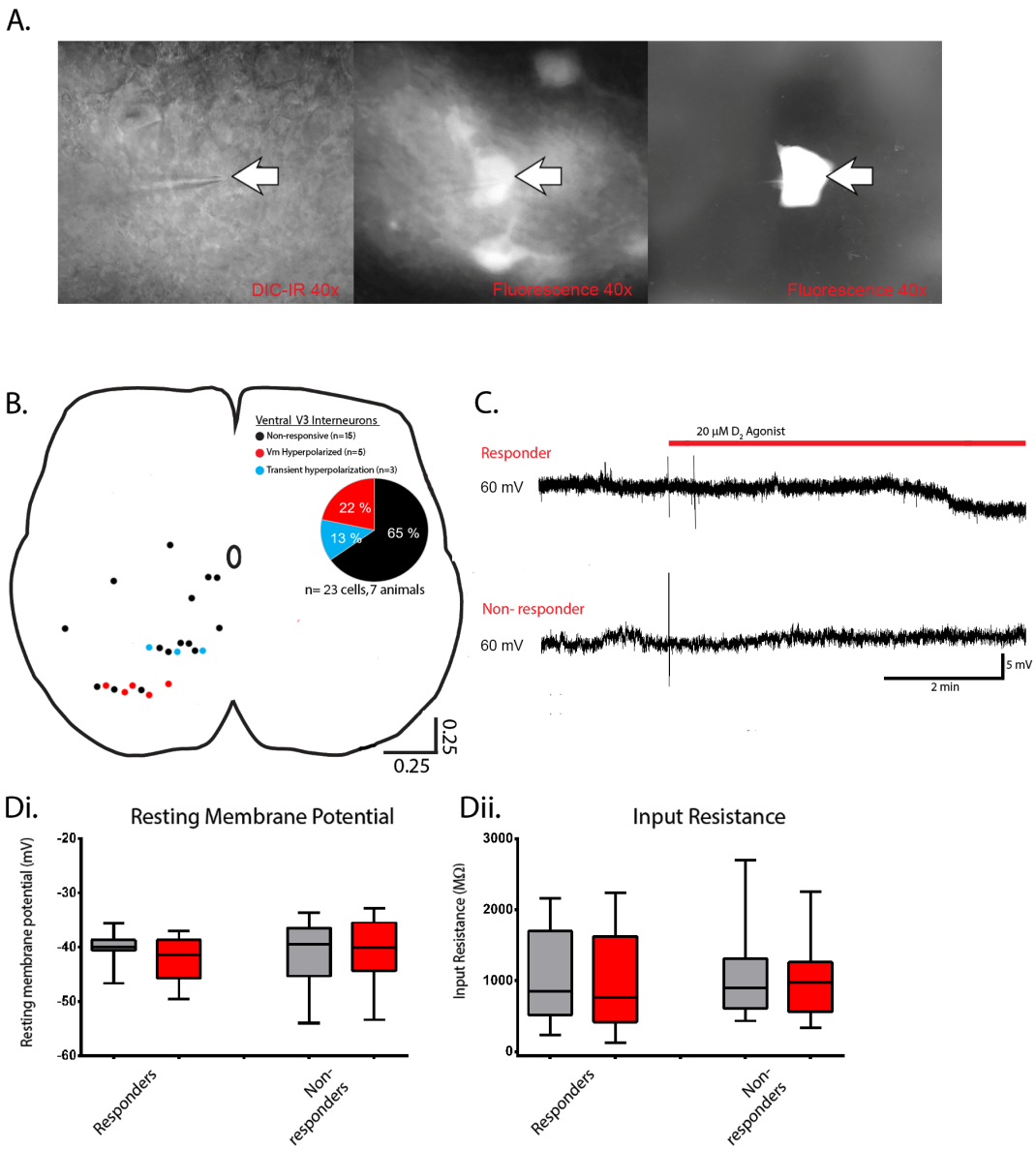

Supplemental Figure 1*: *D_2 - receptor control of V3 interneurons.
Whole-cell patch-clamp recordings obtained from lamina V3 interneurons. A. Visually guided patch showing pipette tip on a GFP labelled-V3 interneuron. B. V3 interneuron location was measured relative to the central canal and X-Y positions normalized to the distance of ventral and lateral borders of lumbar slices. Non-responders represented by black dots, responders by red dots, and transient responders by blue dots. C. A sample trace showing a hyperpolarization of the resting membrane potential following administration of 20 µM quinpirole in responders (top trace) and non-responders (bottom trace). Di. Box and whisker plots showing a change in resting membrane potential in responders and non-responders before (gray) and after (red) administration of quinpirole. Dii. Input resistance graphed in a similar manner as Di.

References

Abbinanti MD, Zhong G, Harris-Warrick RM (2012) Postnatal emergence of serotonin-induced plateau potentials in commissural interneurons of the mouse spinal cord. J Neurophysiol 108:2191–2202.

Acton D, Broadhead MJ, Miles GB (2018) Modulation of spinal motor networks by astrocyte-derived adenosine is dependent on D-like dopamine receptor signaling. J Neurophysiol 120:998–1009.

Barriere G, Mellen N, Cazalets J-R (2004) Neuromodulation of the locomotor network by dopamine in the isolated spinal cord of newborn rat. Eur J Neurosci 19:1325–1335.

Bolton AD, Murata Y, Kirchner R, Kim S-Y, Young A, Dang T, Yanagawa Y, Constantine-Paton M (2015) A Diencephalic Dopamine Source Provides Input to the Superior Colliculus, where D1 and D2 Receptors Segregate to Distinct Functional Zones. Cell Rep 13:1003–1015.

Bonnot A, Morin D, Viala D (1998) Genesis of spontaneous rhythmic motor patterns in the lumbosacral spinal cord of neonate mouse. Brain Res Dev Brain Res 108:89–99.

Borowska J, Jones CT, Deska-Gauthier D, Zhang Y (2015) V3 interneuron subpopulations in the mouse spinal cord undergo distinctive postnatal maturation processes. Neuroscience 295:221–228.

Borowska J, Jones CT, Zhang H, Blacklaws J, Goulding M, Zhang Y (2013) Functional subpopulations of V3 interneurons in the mature mouse spinal cord. J Neurosci 33:18553–18565.

Bos R, Harris-Warrick RM, Brocard C, Demianenko LE, Manuel M, Zytnicki D, Korogod SM, Brocard F (2018) Kv1.2 Channels Promote Nonlinear Spiking Motoneurons for Powering Up Locomotion. Cell Rep 22:3315–3327.

Button DC, Kalmar JM, Gardiner K, Cahill F, Gardiner PF (2007) Spike frequency adaptation of rat hindlimb motoneurons. J Appl Physiol 102:1041–1050.

Butt SJB, Harris-Warrick RM, Kiehn O (2002) Firing properties of identified interneuron populations in the mammalian hindlimb central pattern generator. J Neurosci 22:9961–9971.

Butt SJB, Kiehn O (2003) Functional identification of interneurons responsible for left-right coordination of hindlimbs in mammals. Neuron 38:953–963.

Caldeira V, Dougherty KJ, Borgius L, Kiehn O (2017) Spinal Hb9::Cre-derived excitatory interneurons contribute to rhythm generation in the mouse. Sci Rep 7:41369.

Chopek JW, Nascimento F, Beato M, Brownstone RM, Zhang Y (2018) Sub-populations of Spinal V3 Interneurons Form Focal Modules of Layered Pre-motor Microcircuits. Cell Rep 25:146–156.e3.

Clemens S, Belin-Rauscent A, Simmers J, Combes D (2012) Opposing modulatory effects of D1- and D2-like receptor activation on a spinal central pattern generator. J Neurophysiol 107:2250–2259.

Clemens S, Hochman S (2004) Conversion of the modulatory actions of dopamine on spinal reflexes from depression to facilitation in D3 receptor knock-out mice. J Neurosci 24:11337–11345.

Commissiong JW (1983) Development of catecholaminergic nerves in the spinal cord of the rat. Brain Res 264:197–208.

Dalrymple AN, Sharples SA, Osachoff N, Lognon AP, Whelan PJ (2019) A supervised machine learning

approach to characterize spinal network function. J Neurophysiol 121:2001–2012.

Dietz S, Husch A, Harris-Warrick RM (2012) A comparison of serotonin neuromodulation of mouse spinal V2a interneurons using perforated patch and whole cell recording techniques. Front Cell Neurosci 6:39.

Dougherty KJ, Zagoraiou L, Satoh D, Rozani I, Doobar S, Arber S, Jessell TM, Kiehn O (2013) Locomotor rhythm generation linked to the output of spinal shox2 excitatory interneurons. Neuron 80:920–933.

Dreyer JK, Herrik KF, Berg RW, Hounsgaard JD (2010) Influence of phasic and tonic dopamine release on receptor activation. J Neurosci 30:14273–14283.

Falgairolle M, O'Donovan MJ (2019) Feedback regulation of locomotion by motoneurons in the vertebrate spinal cord. Current Opinion in Physiology Available at: http://dx.doi.org/10.1016/j.cophys.2018.12.009.

GackiÃ¨re F, Vinay L (2014) Serotonergic modulation of post-synaptic inhibition and locomotor alternating pattern in the spinal cord. Front Neural Circuits 8 Available at: http://dx.doi.org/10.3389/fncir.2014.00102.

Garraway SM, Hochman S (2001) Modulatory Actions of Serotonin, Norepinephrine, Dopamine, and Acetylcholine in Spinal Cord Deep Dorsal Horn Neurons. J Neurophysiol 86:2183–2194.

Gordon IT, Whelan PJ (2006) Monoaminergic control of cauda-equina-evoked locomotion in the neonatal mouse spinal cord. J Neurophysiol 96:3122–3129.

Gozal EA, O'Neill BE, Sawchuk MA, Zhu H, Halder M, Chou C-C, Hochman S (2014) Anatomical and functional evidence for trace amines as unique modulators of locomotor function in the mammalian spinal cord. Front Neural Circuits 8:134.

Gutierrez GJ, O'Leary T, Marder E (2013) Multiple mechanisms switch an electrically coupled, synaptically inhibited neuron between competing rhythmic oscillators. Neuron 77:845–858.

Han P, Nakanishi ST, Tran MA, Whelan PJ (2007a) Dopaminergic modulation of spinal neuronal excitability. J Neurosci 27:13192–13204.

Han P, Nakanishi ST, Tran MA, Whelan PJ (2007b) Dopaminergic Modulation of Spinal Neuronal Excitability. Journal of Neuroscience 27:13192–13204.

Han P, Whelan PJ (2009) Modulation of AMPA currents by D1-like but not D2-like receptors in spinal motoneurons. Neuroscience 158:1699–1707.

Hanson MG, Landmesser LT (2003) Characterization of the circuits that generate spontaneous episodes of activity in the early embryonic mouse spinal cord. J Neurosci 23:587–600.

Hanson MG, Landmesser LT (2004) Normal patterns of spontaneous activity are required for correct motor axon guidance and the expression of specific guidance molecules. Neuron 43:687–701.

Humphreys JM, Whelan PJ (2012) Dopamine exerts activation-dependent modulation of spinal locomotor circuits in the neonatal mouse. J Neurophysiol 108:3370–3381.

Husch A, Dietz SB, Hong DN, Harris-Warrick RM (2015) Adult spinal V2a interneurons show increased

excitability and serotonin-dependent bistability. Journal of Neurophysiology 113:1124–1134 Available at: http://dx.doi.org/10.1152/jn.00741.2014.

Husch A, Van Patten GN, Hong DN, Scaperotti MM, Cramer N, Harris-Warrick RM (2012) Spinal Cord Injury Induces Serotonin Supersensitivity without Increasing Intrinsic Excitability of Mouse V2a Interneurons. Journal of Neuroscience 32:13145–13154 Available at: http://dx.doi.org/10.1523/jneurosci.2995-12.2012.

Jay M, De Faveri F, McDearmid JR (2015) Firing dynamics and modulatory actions of supraspinal dopaminergic neurons during zebrafish locomotor behavior. Curr Biol 25:435–444.

Jean-Xavier C, Mentis GZ, O'Donovan MJ, Cattaert D, Vinay L (2007) Dual personality of GABA/glycine-mediated depolarizations in immature spinal cord. Proc Natl Acad Sci U S A 104:11477–11482.

Jiang Z, Carlin KP, Brownstone RM (1999) An in vitro functionally mature mouse spinal cord preparation for the study of spinal motor networks. Brain Res 816:493–499.

Kawamoto K, Otsuguro K, Ishizuka M, Ito S (2012) Inhibitory effects of dopamine on spinal synaptic transmission via dopamine D1-like receptors in neonatal rats. Br J Pharmacol 166:788–800.

Kemnitz CP, Strauss TR, Hosford DM, Buchanan JT (1995) Modulation of swimming in the lamprey, Petromyzon marinus, by serotonergic and dopaminergic drugs. Neurosci Lett 201:115–118.

Kiehn O (2016) Decoding the organization of spinal circuits that control locomotion. Nat Rev Neurosci 17:224–238.

Kiehn O, Butt SJB (2003) Physiological, anatomical and genetic identification of CPG neurons in the developing mammalian spinal cord. Prog Neurobiol 70:347–361.

LaHoste GJ, Marshall JF (1993) The role of dopamine in the maintenance and breakdown of D1/D2 synergism. Brain Res 611:108–116.

Lambert AM, Bonkowsky JL, Masino MA (2012) The conserved dopaminergic diencephalospinal tract mediates vertebrate locomotor development in zebrafish larvae. J Neurosci 32:13488–13500.

Lapointe NP, Rouleau P, Ung R-V, Guertin PA (2009) Specific role of dopamine D1 receptors in spinal network activation and rhythmic movement induction in vertebrates. J Physiol 587:1499–1511.

Lee SP, So CH, Rashid AJ, Varghese G, Cheng R, José Lança A, O'Dowd BF, George SR (2004) Dopamine D1 and D2 Receptor Co-activation Generates a Novel Phospholipase C-mediated Calcium Signal. J Biol Chem 279:35671–35678.

Li Y, Li L, Stephens MJ, Zenner D, Murray KC, Winship IR, Vavrek R, Baker GB, Fouad K, Bennett DJ (2014) Synthesis, transport, and metabolism of serotonin formed from exogenously applied 5-HTP after spinal cord injury in rats. J Neurophysiol 111:145–163.

Madriaga MA, McPhee LC, Chersa T, Christie KJ, Whelan PJ (2004) Modulation of locomotor activity by multiple 5-HT and dopaminergic receptor subtypes in the neonatal mouse spinal cord. J Neurophysiol 92:1566–1576.

Marder E (2012) Neuromodulation of Neuronal Circuits: Back to the Future. Neuron 76:1–11 Available at: http://dx.doi.org/10.1016/j.neuron.2012.09.010.

Marder E, O'Leary T, Shruti S (2014) Neuromodulation of circuits with variable parameters: single neurons and small circuits reveal principles of state-dependent and robust neuromodulation. Annu Rev Neurosci 37:329–346.

Marder E, Thirumalai V (2002) Cellular, synaptic and network effects of neuromodulation. Neural Netw 15:479–493.

McPherson DR, Kemnitz CP (1994) Modulation of lamprey fictive swimming and motoneuron physiology by dopamine, and its immunocytochemical localization in the spinal cord. Neurosci Lett 166:23–26.

Megat S, Shiers S, Moy JK, Barragan-Iglesias P, Pradhan G, Seal RP, Dussor G, Price TJ (2018) A Critical Role for Dopamine D5 Receptors in Pain Chronicity in Male Mice. J Neurosci 38:379–397.

Milan L, Barrière G, De Deurwaerdère P, Cazalets J-R, Bertrand SS (2014) Monoaminergic control of spinal locomotor networks in SOD1G93A newborn mice. Front Neural Circuits 8:77.

Miles GB, Dai Y, Brownstone RM (2005) Mechanisms underlying the early phase of spike frequency adaptation in mouse spinal motoneurones. J Physiol 566:519–532.

Miles GB, Sillar KT (2011) Neuromodulation of vertebrate locomotor control networks. Physiology 26:393–411.

Mor Y, Lev-Tov A (2007) Analysis of rhythmic patterns produced by spinal neural networks. J Neurophysiol 98:2807–2817.

Musienko P, van den Brand R, Märzendorfer O, Roy RR, Gerasimenko Y, Edgerton VR, Courtine G (2011) Controlling specific locomotor behaviors through multidimensional monoaminergic modulation of spinal circuitries. J Neurosci 31:9264–9278.

Myers CP, Lewcock JW, Hanson MG, Gosgnach S, Aimone JB, Gage FH, Lee K-F, Landmesser LT, Pfaff SL (2005) Cholinergic input is required during embryonic development to mediate proper assembly of spinal locomotor circuits. Neuron 46:37–49.

Nakanishi ST, Whelan PJ (2010) Diversification of intrinsic motoneuron electrical properties during normal development and botulinum toxin-induced muscle paralysis in early postnatal mice. J Neurophysiol 103:2833–2845.

Perreault ML, Hasbi A, Alijaniaram M, Fan T, Varghese G, Fletcher PJ, Seeman P, O'Dowd BF, George SR (2010) The dopamine D1-D2 receptor heteromer localizes in dynorphin/enkephalin neurons: increased high affinity state following amphetamine and in schizophrenia. J Biol Chem 285:36625–36634.

Pflieger J-F, Clarac F, Vinay L (2002) Postural modifications and neuronal excitability changes induced by a short-term serotonin depletion during neonatal development in the rat. J Neurosci 22:5108–5117.

Picton LD, Nascimento F, Broadhead MJ, Sillar KT, Miles GB (2017) Sodium Pumps Mediate Activity-Dependent Changes in Mammalian Motor Networks. J Neurosci 37:906–921.

Picton LD, Sillar KT (2016) Mechanisms underlying the endogenous dopaminergic inhibition of spinal locomotor circuit function in Xenopus tadpoles. Sci Rep 6:35749.

Quinlan KA, Kiehn O (2007) Segmental, synaptic actions of commissural interneurons in the mouse spinal cord. J Neurosci 27:6521–6530.

Rashid AJ, So CH, Kong MMC, Furtak T, El-Ghundi M, Cheng R, O'Dowd BF, George SR (2007) D1-D2 dopamine receptor heterooligomers with unique pharmacology are coupled to rapid activation of Gq/11 in the striatum. Proc Natl Acad Sci U S A 104:654–659.

Rashid AJ, So CS, O'Dowd BF, George SR (2006) S.19.05 Heterooligomerization of D1 and D2 dopamine receptors in brain: implications for psychosis? Eur Neuropsychopharmacol 16:S193.

Reimer MM, Norris A, Ohnmacht J, Patani R, Zhong Z, Dias TB, Kuscha V, Scott AL, Chen Y-C, Rozov S, Frazer SL, Wyatt C, Higashijima S-I, Patton EE, Panula P, Chandran S, Becker T, Becker CG (2013) Dopamine from the brain promotes spinal motor neuron generation during development and adult regeneration. Dev Cell 25:478–491.

Ren J, Greer JJ (2003) Ontogeny of rhythmic motor patterns generated in the embryonic rat spinal cord. J Neurophysiol 89:1187–1195.

Ren L-Q, Wienecke J, Hultborn H, Zhang M (2016) Production of Dopamine by Aromaticl-Amino Acid Decarboxylase Cells after Spinal Cord Injury. J Neurotrauma 33:1150–1160.

Restrepo CE, Lundfald L, Szabó G, Erdélyi F, Zeilhofer HU, Glover JC, Kiehn O (2009) Transmitter-phenotypes of commissural interneurons in the lumbar spinal cord of newborn mice. J Comp Neurol 517:177–192.

Rivera-Oliver M, Moreno E, Álvarez-Bagnarol Y, Ayala-Santiago C, Cruz-Reyes N, Molina-Castro GC, Clemens S, Canela EI, Ferré S, Casadó V, Díaz-Ríos M (2018) Adenosine A-Dopamine D Receptor Heteromers Control the Excitability of the Spinal Motoneuron. Mol Neurobiol Available at: http://dx.doi.org/10.1007/s12035-018-1120-y.

Schotland J, Shupliakov O, Wikström M, Brodin L, Srinivasan M, You ZB, Herrera-Marschitz M, Zhang W, Hökfelt T, Grillner S (1995) Control of lamprey locomotor neurons by colocalized monoamine transmitters. Nature 374:266–268.

Sharples SA (2017) Dopamine Pumping Up Spinal Locomotor Network Function. J Neurosci 37:3103–3105.

Sharples SA, Humphreys JM, Jensen AM, Dhoopar S, Delaloye N, Clemens S, Whelan PJ (2015) Dopaminergic modulation of locomotor network activity in the neonatal mouse spinal cord. J Neurophysiol 113:2500–2510.

Sharples SA, Koblinger K, Humphreys JM, Whelan PJ (2014) Dopamine: a parallel pathway for the modulation of spinal locomotor networks. Front Neural Circuits 8:55.

Sharples SA, Whelan PJ (2017) Modulation of Rhythmic Activity in Mammalian Spinal Networks Is Dependent on Excitability State. eNeuro 4 Available at: http://dx.doi.org/10.1523/ENEURO.0368-16.2017.

Smith JC, Feldman JL (1987) In vitro brainstem-spinal cord preparations for study of motor systems for mammalian respiration and locomotion. J Neurosci Methods 21:321–333.

Stein W (2009) Modulation of stomatogastric rhythms. J Comp Physiol A Neuroethol Sens Neural Behav Physiol 195:989–1009.

Svensson E, Wikström MA, Hill RH, Grillner S (2003) Endogenous and exogenous dopamine presynaptically inhibits glutamatergic reticulospinal transmission via an action of D2-receptors on N-type Ca2+ channels. Eur J Neurosci 17:447–454.

Thirumalai V, Cline HT (2008) Endogenous dopamine suppresses initiation of swimming in prefeeding zebrafish larvae. J Neurophysiol 100:1635–1648.

Thompson JL, Yang J, Lau B, Liu S, Baimel C, Kerr LE, Liu F, Borgland SL (2016) Age-Dependent D1-D2 Receptor Coactivation in the Lateral Orbitofrontal Cortex Potentiates NMDA Receptors and Facilitates Cognitive Flexibility. Cereb Cortex 26:4524–4539.

Ugrumov MV, Saifetyarova JY, Lavrentieva AV, Sapronova AY (2012) Developing brain as an endocrine organ: Secretion of dopamine. Mol Cell Endocrinol 348:78–86.

Wang D, Grillner S, Wallén P (2011) 5-HT and dopamine modulates CaV1.3 calcium channels involved in postinhibitory rebound in the spinal network for locomotion in lamprey. J Neurophysiol 105:1212–1224.

Warp E, Agarwal G, Wyart C, Friedmann D, Oldfield CS, Conner A, Del Bene F, Arrenberg AB, Baier H, Isacoff EY (2012) Emergence of patterned activity in the developing zebrafish spinal cord. Curr Biol 22:93–102.

Whelan P, Bonnot A, O'Donovan MJ (2000a) Properties of rhythmic activity generated by the isolated spinal cord of the neonatal mouse. J Neurophysiol 84:2821–2833.

Whelan P, Bonnot A, O'Donovan MJ (2000b) Properties of rhythmic activity generated by the isolated spinal cord of the neonatal mouse. J Neurophysiol 84:2821–2833.

Wienecke J, Ren L-Q, Hultborn H, Chen M, Møller M, Zhang Y, Zhang M (2014) Spinal cord injury enables aromatic L-amino acid decarboxylase cells to synthesize monoamines. J Neurosci 34:11984–12000.

Zhang Y, Narayan S, Geiman E, Lanuza GM, Velasquez T, Shanks B, Akay T, Dyck J, Pearson K, Gosgnach S, Fan C-M, Goulding M (2008) V3 spinal neurons establish a robust and balanced locomotor rhythm during walking. Neuron 60:84–96.

Zhong G, Díaz-Ríos M, Harris-Warrick RM (2006) Intrinsic and functional differences among commissural interneurons during fictive locomotion and serotonergic modulation in the neonatal mouse. J Neurosci 26:6509–6517.

Zhu H, Clemens S, Sawchuk M, Hochman S (2007) Expression and distribution of all dopamine receptor subtypes (D(1)-D(5)) in the mouse lumbar spinal cord: a real-time polymerase chain reaction and non-autoradiographic in situ hybridization study. Neuroscience 149:885–897.